Vilnius University
Faculty of Physics
Institute of Photonics and Nanotechnology

Aivaras Špokas

OPTIMIZATION OF ELECTRICALLY PUMPED GaAsBi EMITTERS FOR NEAR INFRARED OPERATION

Master's final thesis

Photonics and Nanotechnology study programme

Student	Aivaras Špokas
Approved	2026-05-20
Academic Supervisor	Assoc. Prof. Dr. Renata Butkutė
Director of the Institute	Prof. Dr. Ramūnas Aleksiejūnas

Vilnius 2026

Vilniaus universiteto
Fizikos fakulteto
Fotonikos ir nanotechnologijų institutas

Aivaras Špokas

ELEKTRIŠKAI KAUPINAMŲ NIR GaAsBi EMITERIŲ TECHNOLOGIJOS OPTIMIZAVIMAS

Magistrantūros studijų baigiamasis darbas

Fotonikos ir nanotechnologijų studijų programa

Studentas	Aivaras Špokas
Leista ginti	2026-05-20
Mokslinis vadovas	doc. dr. Renata Butkutė
Instituto direktorius	prof. dr. Ramūnas Aleksiejūnas

Vilnius 2026

Contents

List of Abbreviations

AFM atomic force microscopy

BEP beam equivalent pressure

BEPR beam equivalent pressure ratio

CW continuous-wave

DIC differential interference contrast

E-band extended band

EDX energy dispersive X-ray spectroscopy

EL electroluminescence

FWHM full width at half maximum

HRXRD high-resolution X-ray diffraction

HT high temperature

I_{th} threshold current

LD laser diode

LED light-emitting diode

LT low temperature

LTG low-temperature grown

MBE molecular beam epitaxy

MOVPE metal-organic vapor-phase epitaxy

MQW multiple quantum well

NIR near-infrared

O-band original band

PL photoluminescence

PQW parabolic quantum well

QD quantum dot

QW quantum well

RHEED reflection high energy electron diffraction

RSM reciprocal space mapping

RT room-temperature

SEM scanning electron microscope

SPM scanning probe microscopy

SQW single quantum well

STEM scanning transmission electron microscopy

TD temperature-dependent

TST two substrate temperature

XRD X-ray diffraction

Introduction

The development of efficient near-infrared (NIR) semiconductor emitters relies not only on mature material systems, but also on the ability to engineer novel solutions, including metastable alloys and 2D material systems, that extend the available spectral range while remaining compatible with established semiconductor platforms. Classical III-V compounds such as GaAs, AlGaAs, InGaAs, and InP already cover a large part of the optoelectronic device market. Nevertheless, the spectral region around 1000-1300 nm remains technologically challenging. InGaAs structures grown on GaAs can reach this range only by introducing large In contents, which increases strain and can lead to relaxation and misfit dislocation formation. On the other hand, InP-based materials are usually more suitable for longer wavelength emission. Therefore, alternative GaAs-compatible material systems are required for efficient emitters operating in this transitional NIR range.

Metastable semiconductor alloys provide a route to overcome some of these limitations, because they can introduce strong band-structure modifications that are not accessible in conventional compounds. However, the same non-equilibrium nature that makes such alloys useful also makes them difficult to grow reproducibly. Their epitaxy is governed by a delicate balance between incorporation, segregation, desorption, defect formation, and phase separation. As a result, the growth conditions that produce good crystalline quality in the host material are often not directly suitable for the metastable alloy. Instead, high optical quality is usually obtained only within a narrow interval of substrate temperature, growth rate, and material fluxes.

GaAsBi is one of the most promising examples of such a material system for NIR optoelectronics. Replacing a small fraction of As atoms by Bi in the GaAs lattice produces a large bandgap reduction, with reported values reaching up to 88 meV/%Bi [1]. This allows long-wavelength emission to be obtained while introducing a smaller lattice mismatch than in highly strained InGaAs/GaAs structures. In addition, Bi incorporation strongly affects the valence band and increases the spin-orbit split-off energy. At sufficiently large Bi contents, the spin-orbit split-off energy can become larger than the band gap, making the CHSH Auger recombination process energetically unfavourable [2]. GaAsBi also shows a reduced temperature dependence of the emission energy, which is attractive for devices intended to operate under varying environmental conditions [3, 4].

These properties make GaAsBi an attractive active-region material for light-emitting diodes (LEDs) and laser diodes (LDs) in the NIR. One application where this wavelength range is important is reflectance-mode pulse oximetry. Conventional pulse oximetry commonly relies on red and NIR wavelengths, but in reflectance geometry the different penetration depths of the two wavelengths reduce measurement accuracy. A possible solution is to use two NIR emitters, for example near 800 nm and 1100 nm, where the optical penetration depths in tissue are more similar. AlGaAs-based emitters can provide the shorter wavelength, whereas GaAsBi is a promising candidate for the longer-wavelength source on the GaAs platform [5].

Despite these advantages, the wider application of GaAsBi is limited by its complicated growth. Bi is considerably larger than As, has low solubility in GaAs, and tends to segregate at the growth surface. Bi incorporation generally requires low substrate temperatures and an As/Ga ratio close to the stoichiometric boundary [6, 7]. Excessive As flux suppresses Bi incorporation because As competes with Bi for group-V lattice sites. In contrast, insufficient As flux can lead to Ga-rich growth, droplet formation, rough morphology, and thickness non-uniformity. These conditions are further complicated by the fact that the low temperatures required for Bi incorporation promote the formation of point defects associated with both GaAsBi and low-temperature-grown GaAs [8, 9].

Consequently, the main challenge is not only to incorporate Bi into GaAs, but to do so reproducibly while maintaining sufficient crystalline and optical quality. This is especially important for electrically pumped devices, where the active region is surrounded by doped carrier transport and optical confinement layers. Defects introduced either in the GaAsBi active region or in the surrounding low-temperature-grown layers can increase non-radiative recombination, current leakage, and local heating. Although GaAsBi-based LEDs and LDs have already been demonstrated, their performance and reproducibility remain limited compared with more mature III-V emitters.

Most GaAsBi growth optimization has therefore focused on identifying a narrow near stoichiometric growth window. However, the exact numerical values of the optimal beam equivalent pressure ratio (BEPR) are strongly dependent on the geometry and calibration of each molecular beam epitaxy (MBE) system. Moreover, growth behaviour can differ substantially between thick layers, thin quantum wells (QWs), and full diode structures. Thick layers provide a clearer view of alloy formation, droplet development, composition uniformity, and strain, while QWs are more directly relevant for efficient emitters but are highly sensitive to interface quality, segregation, and transient growth effects. A more comprehensive investigation must therefore include both layer growth and QW-based device structures.

This work focuses on the optimization of GaAsBi growth and its transfer into electrically pumped NIR emitters. First, GaAsBi layers were grown over a wide As/Ga BEPR range in order to clarify whether useful growth regimes exist outside the commonly accepted near-stoichiometric window. The structural, morphological, and optical properties of these layers were investigated to determine how the As/Ga and Bi/Ga flux balance affects Bi incorporation, droplet formation, layer thickness, and emission properties. Particular attention was given to identifying growth regimes that could be useful for thin active regions, even if they are not ideal for thick homogeneous layers.

The second part of the work transferred the most promising growth conditions into GaAsBi QWs for applications in LED, and LD structures. The QW growth was optimized for NIR emission in the range relevant to GaAsBi-based emitters, while several device configurations were investigated to evaluate the technological flexibility of the developed approach. This included standard and flipped diode architectures, structures grown on AlAs sacrificial layers for future substrate removal and integration, and active-region designs with improved carrier confinement. In this way, the work connects fundamental growth-window optimization with the practical requirements of electrically pumped GaAsBi emitters. Therefore, **the goal of this thesis** is twofold:

1. To investigate GaAsBi layer growth by MBE over an extended range of technological conditions and identify the regimes that provide favourable optical properties for NIR emitter applications.

2. To apply the optimized GaAsBi growth conditions to QW-based structures and fabricate electrically pumped NIR LEDs and LDs.

To achieve this goal, the following tasks were formulated:

1. To investigate GaAsBi layer growth over an extended As/Ga BEPR range and identify growth regimes with enhanced optical properties, suitable for NIR optoelectronic applications.
2. To evaluate the influence of As/Ga and Bi/Ga flux balance on Bi incorporation, layer thickness, surface morphology, and optical quality.
3. To select the most promising growth regime for GaAsBi QW structures and optimize their emission properties.
4. To grow and characterize GaAsBi-based LDs and LEDs in integration-ready device configurations, including flipped diode structures on AlAs sacrificial layers.
5. To fabricate and characterize GaAsBi-based LDs and evaluate the influence of active-region design on device performance.

1 Literature Review

1.1 Properties of GaAsBi

The investigation into GaAsBi is mainly driven by its attractive properties for NIR emitters. In current NIR systems the detector market is well developed, but there are serious bottlenecks in the emitter market. The major issues are caused by the large Auger recombination losses associated with narrow band gap semiconductors. In addition, the high cooling requirements decrease the wall-plug-efficiency of said devices. GaAsBi could be a solution for both of these drawbacks. First of all, it has been showcased that GaAsBi LDs can operate in room-temperature (RT), mitigating the need for costly cooling solutions [4]. Moreover, in the first report of the GaAsBi alloy by *Oe and Okamoto* it was noticed that the emission wavelength dependence on temperature is weaker when compared to other III-V semiconductor emitters. The report stated that, for a GaAsBi layer with a 2.4% Bi content, the photoluminescence (PL) peak position variation with temperature was around 0.1 meV/K [3]. This shows another advantage of this alloy for applications of GaAsBi-based emitters in a wide range of environmental conditions. Beyond these temperature-related benefits, the interest into GaAsBi is strongly influenced by the ability to reduce non-radiative recombination losses. It was shown that at a Bi content of around 10.5% the spin-orbit split-off (ΔSO) surpasses band gap (E_g) (see Fig. 1) [2, 10]. This band-structure crossover provides a possibility to suppress losses related to Auger recombination and inter-valence band absorption, showing a pathway to more efficient NIR devices [11].

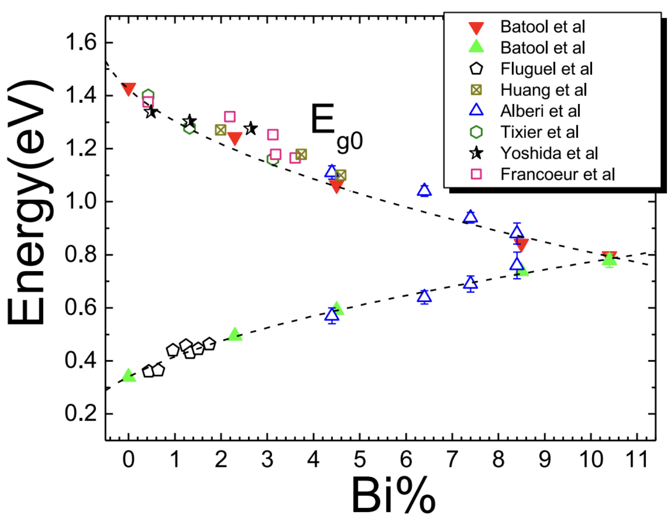

Fig. 1. Dependence of the band-gap energy and spin-orbit split-off energy on Bi content. The crossover point can be observed between 10 and 11 Bi %. Colored symbols represent experimental results, dashed lines correspond to theoretical calculations. Adapted from [10].

On the other hand, the use of GaAsBi also enables more flexibility in emission wavelengths. The strong perturbation of the band structure induced by Bi incorporation causes a large value of band gap reduction, as much as 88 meV/%Bi [1]. This property enables long wavelength emitters grown directly on GaAs substrates, as substitution of a small amount of host lattice element As by

Bi provides a large reduction in band gap, without inducing sufficient strain for formation of misfit dislocations. This is particularly clear when compared to the classical material InGaAs, used for NIR emitters grown on the GaAs platform.

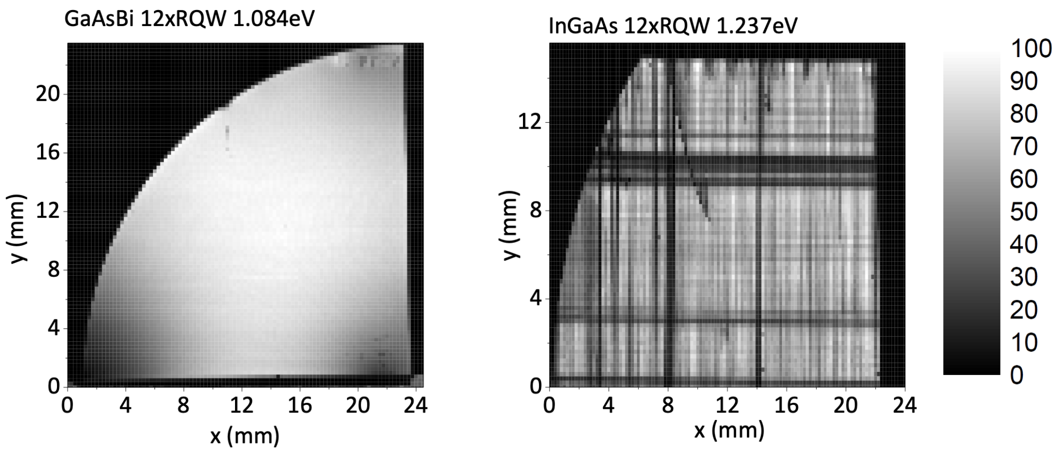

Fig. 2. Comparison of RT PL intensity mapping of GaAsBi (≈ 10 %Bi, scanned at the peak energy of 1.084 eV) and InGaAs (≈ 26 %In, scanned at the peak energy of 1.237 eV) 12×RQW samples. Adapted from [12, 13].

Fig. 2 shows that misfit dislocations are already formed in InGaAs multiple quantum well (MQW) structures emitting at around 1000 nm, while for GaAsBi MQWs high PL homogeneity is achieved even at around 1100 nm, confirming the absence of lattice mismatch dislocations [12].

1.2 Growth of GaAsBi

The wider application of GaAsBi in the next-generation of NIR emitters is held back by the challenging growth of this alloy. Up to this point it has generally been considered that to ensure Bi incorporation and achieve good crystallinity, one must operate in a very narrow window of growth conditions. This narrow growth window originates from the highly metastable nature of GaAsBi. The incorporation of Bi into GaAs is difficult because Bi is considerably larger than As, has low solubility in GaAs, and forms relatively weak Ga–Bi bonds compared with the preferential Ga–As bonding of the host lattice. This necessitates rather unusual growth conditions in GaAsBi. The first is the requirement for low-temperature growth. It was reported by *Richards et al.* that the Bi incorporation threshold is 440 °C (see Fig. 3). Moreover, to incorporate larger fractions of Bi the temperature has to be further reduced, as maximum incorporation scales linearly with substrate temperature [6]. This condition enables the so-called temperature-limited growth regime of GaAsBi, where, if a sufficient Bi flux is supplied, the incorporation becomes governed by the substrate temperature [6, 14]. While this has been shown to be an efficient growth strategy to grow structures with large Bi contents [13], the temperature limitation is a great difficulty as it promotes the formation of point defects associated with both GaAsBi and low-temperature grown (LTG) GaAs, thereby reducing emission efficiency [8,15]. *Štaupienė et al.* showed that this large density of point defects causes trap assisted Auger recombination, resulting in low internal quantum efficiency of GaAsBi [9].

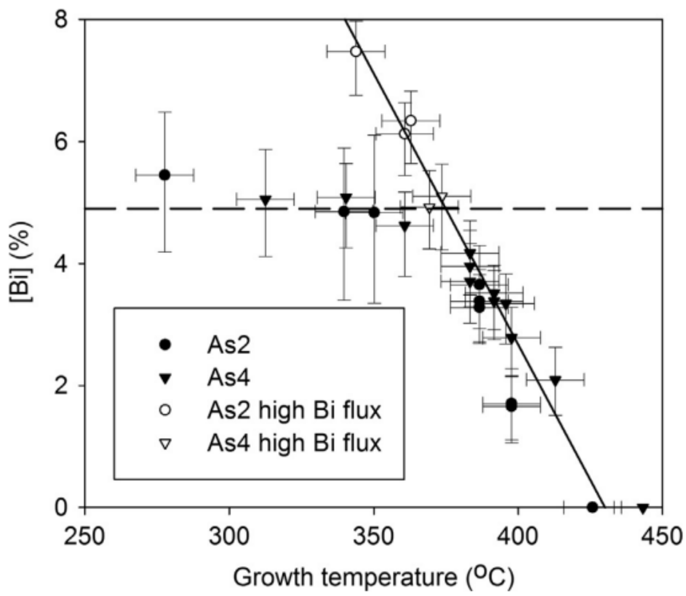

Fig. 3. Dependence of Bi content on the MBE growth temperature in GaAsBi layers grown at Ga to As atomic flux ratio close to unity. Triangles illustrate samples grown with tetrameric arsenic, circles correspond to the use of dimeric As. Solid experimental points are obtained using a low Bi flux, open symbols show growth with increased Bi flux, where the growth is purely temperature-limited. Taken from [6].

The second major challenge is the careful control of the As to Ga flux ratio. In conventional GaAs MBE, growth is typically carried out under As-rich conditions, where the growth rate is typically Ga limited. Such conditions are crucial to achieve good crystal quality. In GaAsBi, however, excessive As flux can suppress Bi incorporation, as Bi competes with As for incorporation into the group-V lattice sites. On the other hand, insufficient As flux results in Ga-rich growth, which can cause surface degradation, and the formation of metallic droplets (see Fig. 4). Thus, it is widely accepted that GaAsBi growth requires a narrow As/Ga window in which sufficient As is supplied to preserve crystalline quality, while avoiding conditions that suppress Bi incorporation [6, 7].

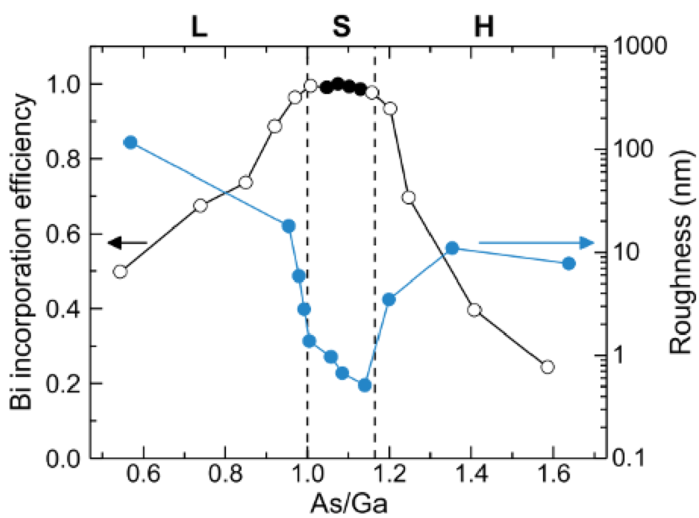

Fig. 4. Dependence of surface roughness and Bi incorporation efficiency on the As to Ga ratio. Taken from [7].

Because the optimum growth window is strongly dependent on the specific MBE system, direct comparison of As/Ga ratios between different studies is not straightforward. Most reports specify the As to Ga ratio in terms of BEPR, rather than absolute atomic flux ratio. However, BEPR is sensitive to factors such as system geometry, ion gauge position, and source configuration. As a result, the same atomic As/Ga flux ratio may correspond to different reported BEPR values in different systems, meaning that the optimum growth conditions are often determined empirically for each reactor. Taken together, these constraints remain a major barrier to the industrial implementation of GaAsBi-based emitters, as the narrow growth window, high defect density, and limited reproducibility between growth systems make device commercialization particularly challenging.

1.2.1 Growth of GaAsBi Layers

Early GaAsBi studies were mainly focused on thick layers. The metastable nature of this alloy not only promotes point-defect formation, but also strongly affects surface morphology. Bi tends to segregate and agglomerate at the growth surface. Combined with the As-poor conditions required for GaAsBi growth, this can produce a variety of surface features related to imbalanced growth conditions. Thick layers are particularly useful for studying these effects, because the longer growth time allows sufficient agglomeration, and droplet formation that can be used to clarify the growth condition window by investigating surface features. A detailed investigation of surface features was published by *Carter et al.*, where a wide range of As, Ga and Bi flux ratios were investigated, focusing on their influence on the surface features of 500 nm thick GaAsBi layers [16].

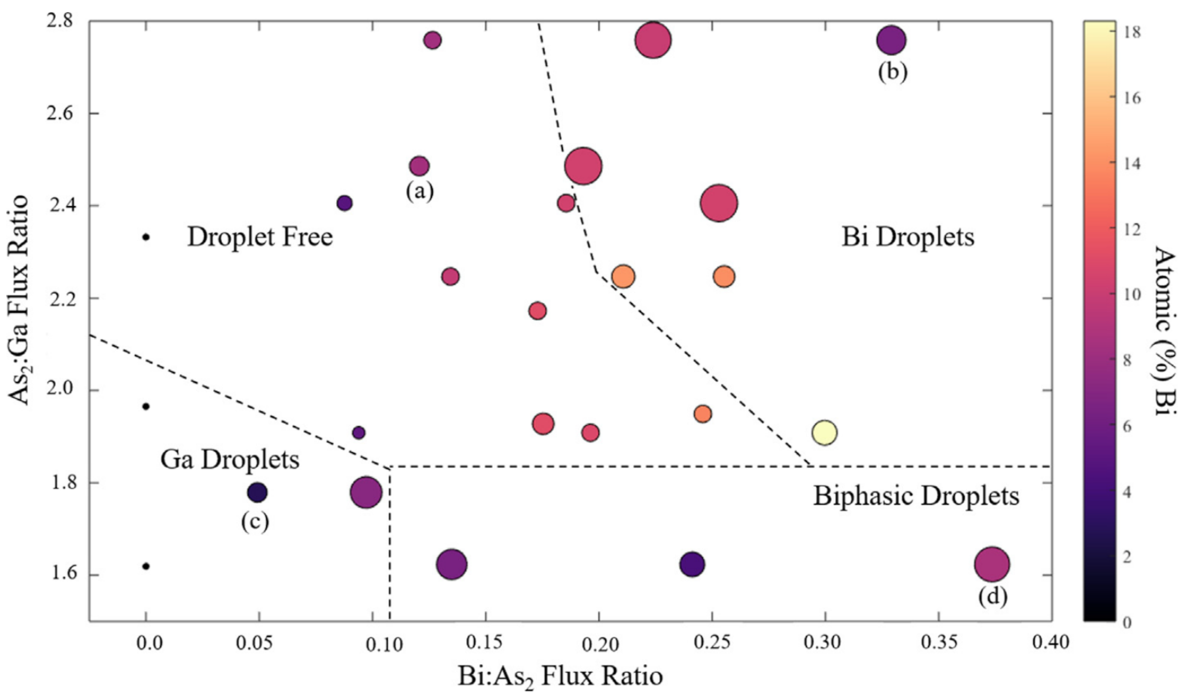

Fig. 5. Technological condition map of surface feature dependence on Ga, As, and Bi flux ratios. The color of the symbols shows the Bi content in the structures. Taken from [16].

It was shown that, to achieve high quality, one must find a balance not only in the As to Ga ratio but also in the Bi flux. The general trends observed were that insufficient As promotes Ga droplet formation, which evolves into a biphasic droplet region when the Bi flux becomes higher than optimal. It is also seen in Fig. 5 that, when operating in the optimal As/Ga region, a droplet-free surface can be achieved; nonetheless, increasing the Bi flux can promote the formation of pure Bi agglomerates. Moreover, the largest Bi incorporation was only achieved for samples with Bi droplets. Similar results were also published by other groups, though it must be noted that droplet free samples were achieved at very different As to Ga beam equivalent pressure (BEP) ratios. *Tominaga et al.* reported smooth surface at BEP As to Ga of around 10, while *Vardar et al.* showed droplet free morphology at a BEPR of 7.5 [17, 18]. This highlights the high dependence on the equipment when considering source BEPs.

However, the presence of droplets not only affects the surface, but it can also hinder the structural homogeneity of the layer itself. Several studies on GaAsBi and AlGaAsBi reported Bi content inhomogeneities caused by self-aligned nanotracks [16, 19–22]. *Wood et al.* provided one of the first structural observations of such features (see Fig. 6) [19].

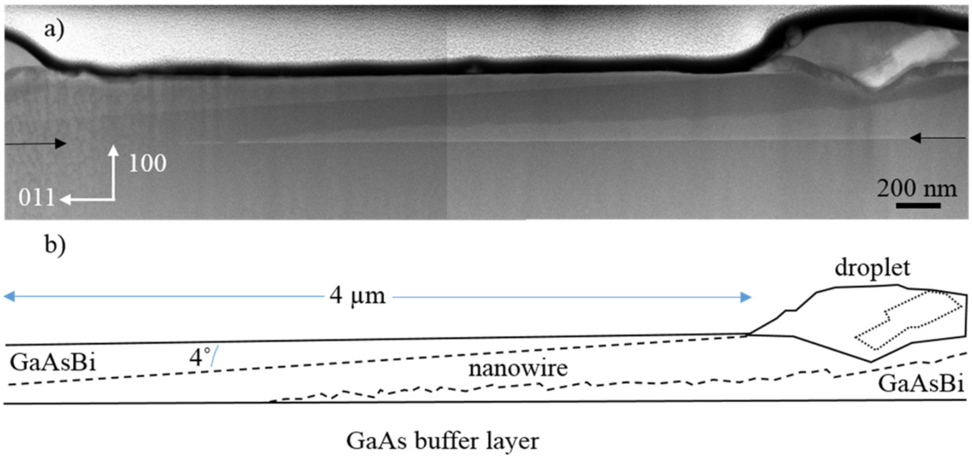

Fig. 6. a) scanning transmission electron microscopy (STEM) image of the self-aligned GaAs nanotrack embedded in a GaAsBi layer, b) schematic representation of the main microstructural features. Taken from [19].

The formation of these nanotracks is generally understood as a droplet-mediated process. There is no common consensus on the exact mechanism causing these nanotracks. *Steele et al.* proposed that the process is initiated by the presence of a Bi droplet that induces a vapour-liquid-solid growth mode [20]. On the other hand, *Wood et al.* and *Tait et al.* attribute the initiation of such compositional inhomogeneities to Ga droplets [19, 21]. Nevertheless, all studies illustrate a broader point, confirming that droplet formation during growth of GaAsBi can cause compositional fluctuations in the structure.

Reyes et al. showed that Bi incorporation can be thickness dependent. It was shown that in the first 25 nm of the growth the Bi content decreases exponentially, after this critical thickness it becomes homogeneous (see Fig. 7) [23]. It is supposed that such growth peculiarity could be the cause of asymmetric PL signal, and consequently, be responsible for the large full width at half maximum (FWHM) of emission from GaAsBi layers.

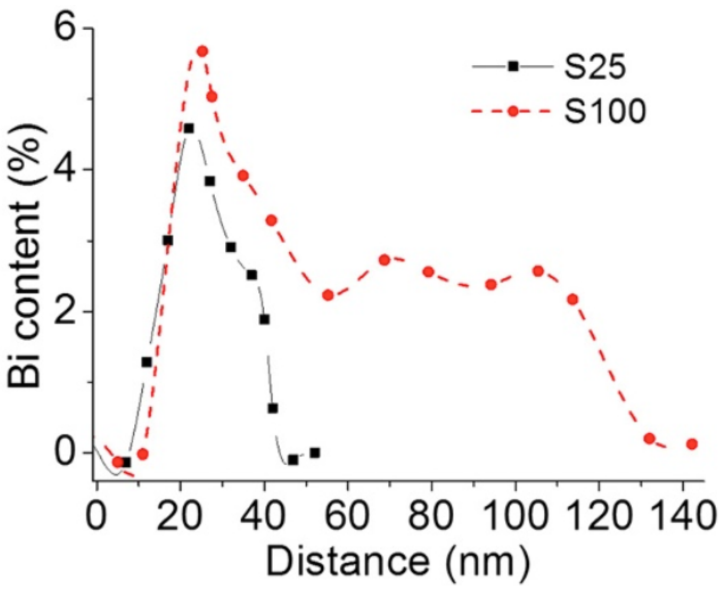

Fig. 7. Evolution of Bi content in GaAsBi layer of two different thicknesses (S25 - 25 nm and S100 - 100 nm). Taken from [23].

The final noteworthy growth peculiarity of GaAsBi layers is related to the strain introduced when As is substituted with the considerably larger Bi atom. *Stevens et al.* showed that growth on relaxed InGaAs buffer layers ([In] 10.5 %) helped to avoid surface droplets and resulted in a larger Bi content incorporated [24].

1.2.2 Growth of GaAsBi Quantum Wells

Many of the discussed issues related to the growth of GaAsBi layers are less prominent, when the thickness is reduced. Thus, choosing to grow GaAsBi QWs is logical both in avoiding drawbacks related to thickness and, when considering applications, where QW devices possess lower pumping thresholds, and higher spectral quality. Nonetheless, the growth of GaAsBi MQWs has its own challenges. According to GaAsBi growth model proposed by *Lu et al.*, Bi atoms are incorporated from a Bi-rich surface layer (wetting layer) (see Fig. 8) [25].

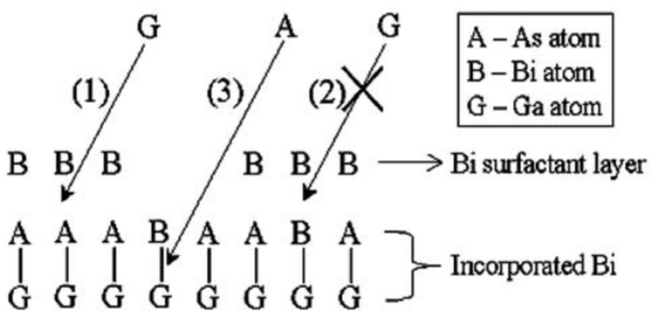

Fig. 8. Proposed GaAsBi growth mechanism under Bi-rich surface conditions. The numbered steps indicate: (1) incorporation of a Ga atom into an As-terminated surface, forming an As–Ga–Bi bonds; (2) suppression of Ga incorporation above Bi-occupied sites, since Bi–Ga–Bi bond formation is unfavorable due to the large atomic size of Bi; and (3) replacement of Bi by an incoming As atom, which breaks the Ga–Bi bond and ejects Bi back to the surface wetting layer. Adapted from [25].

Careful control of this wetting layer is required to achieve good quality of GaAsBi MQW structures. As shown by *Ludewig et al.*, the absence of prior wetting results in the delayed incorporation of Bi, meaning that the first QW in an MQW structure is effectively thinner [26]. Furthermore, as GaAsBi has to be grown at low temperature, usually this same temperature is also used to grow GaAs barriers, adding more defects related to LTG GaAs. In addition to that, Bi segregation into the barrier is also a prominent issue. Since Bi incorporation is surface driven, simply closing the Bi shutter does not terminate the formation of GaAsBi alloy, the segregated surface Bi layer still contributes during the barrier growth. *Patil et al.* proposed a two substrate temperature (TST) growth technique which can aid in limiting this Bi segregation resulting in sharper interfaces, by removing the residual Bi during the elevated temperature growth of the GaAs barrier [27–29]. A study by *Dudutienė et al.* generally agrees with the findings stating that TST growth improves interfaces, enhances Bi compositional homogeneity, lowers carrier localization, and even increases the Bi incorporation efficiency into the GaAsBi lattice [30]. On the other hand, the study also showed that the elevated temperature reduces the residual Bi layer, consequently re-enabling the delayed incorporation discussed by *Ludewig et al.*, and resulting in a large fluctuation of QW thickness (see Fig. 9) [26, 30]. These studies show, that while TST growth has many advantages, the issues in QW homogeneity, that can arise, could be a detrimental drawback, when considering device applications.

Another QW growth peculiarity is related to the design of the quantum structure. It has been shown by *Pūkienė et al.* that by changing the barrier design from classical rectangular to parabolic, one can increase the PL intensity by more than 50 times [31]. Parabolic quantum wells (PQWs) are less attractive due to their intricate growth, despite this they are very relevant when considering devices. A further study has shown that the use of PQW gain region in electrically pumped NIR LDs enhances their properties in terms of output power and threshold current (I_{th}) [5].

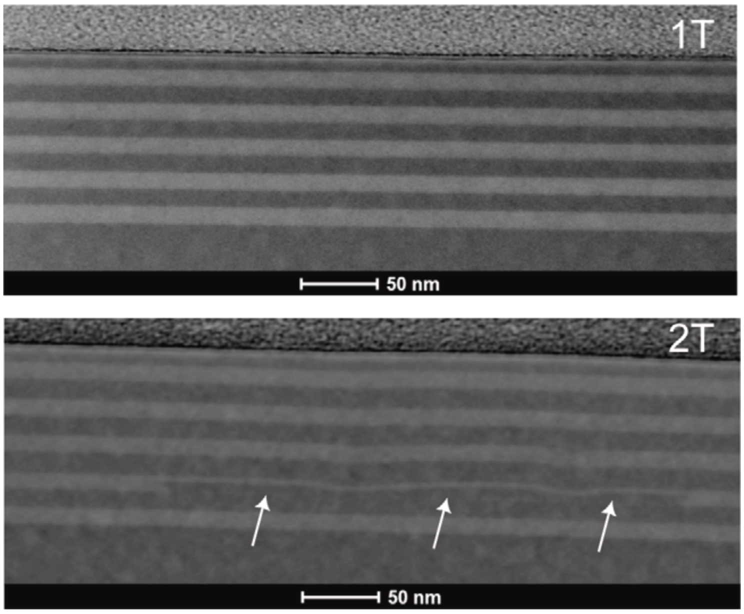

Fig. 9. Comparison of GaAsBi MQW samples growth at a single temperature regime (top), and TST mode (bottom). Darker regions in the micrographs correspond to GaAs, brighter - to GaAsBi. Arrows point to reduced QW thickness attributed to insufficient Bi wetting. Taken from [30].

1.3 GaAsBi Devices

Despite the significant advantages of GaAsBi discussed in subsection 1.1, there has been limited effort in fabrication of GaAsBi-based emitters. This is caused by the difficult growth discussed in the last subsection. Nonetheless, several works have made prototypes showcasing the applicability of GaAsBi. In this section some of the notable works will be reviewed.

The first lasing from a GaAsBi active region was demonstrated by *Tominaga et al.*, more than a decade after the first growth of the alloy itself. The study reported RT lasing by photo-pumping from a Fabry-Perot cavity formed from a semiconductor chip, where the gain region was 390 nm GaAsBi layer with 2.5 % Bi [4]. Three years later *Ludewig et al.* were the first to demonstrate lasing from a diode type laser. The metal-organic vapor-phase epitaxy (MOVPE) grown GaAsBi single quantum well (SQW) structure with 2.2 % of Bi demonstrated RT lasing by pulsed electrical injection at 947 nm [32]. Being the first electrically pumped laser, this showed promise for industrial applications, nonetheless due to the large defect density in GaAsBi, continuous-wave (CW) operation was not realized, while the pulsed pumping also had a very large lasing threshold. A year later, a work by the same group, showed the possibility to enhance the performance by using AlGaAs barriers instead of GaAs, the improvement in optical and electrical confinement allowed to decrease the I_{th} [33]. In 2017 *Wu et al.* achieved CW lasing at 273 K from a structure with a GaAsBi SQW containing 5.8 % Bi [34]. The same report demonstrated the longest RT lasing wavelength from a Fabry-Perot type LD to this day, recorded at 1142 nm, operating at pulsed electrical injection. *Špokas et al.* reported lasing in the range from 1025 nm to 1106 nm. Notably, the research built on the ideas of barrier engineering for enhanced properties, where use of AlGaAs (30 % Al) PQW barriers resulted in doubling of the maximum output power and cutting the I_{th} value in half [5]. *Liu et al.* reported lasing in the telecommunication original band (O-band). The fabricated microdisk lasers with a GaAsBi SQW (5.8 % Bi), were capable of RT CW operation in the spectral range of 1276 - 1407 nm, almost fully covering the O-band and even most of the extended band (E-band) [35]. While the fabrication of microdisk lasers requires intricate processing and is hardly scalable for industrial applications, this shows the capability of achieving emission wavelengths applicable for telecommunications using silica-based fiber networks.

The investigation into lasers is mainly driven by the need for better emitters for telecommunication applications, nevertheless some investigations into LED devices were carried out in parallel. As LEDs are easier device structures requiring fewer processing steps, they are useful for investigating electrical pumping of the GaAsBi active area. In 2009, a year before the first demonstration of lasing, *Lewis et al.* showed the first GaAsBi-based electrically pumped emitter. electroluminescence (EL) with a peak wavelength of 987 nm was demonstrated from a p-i-n diode, with a 50 nm GaAsBi intrinsic layer containing 1.8 % of Bi [36]. Later studies on QW-based LEDs showed the ability to achieve wavelengths over the 1200 nm mark, serving as a proof of concept for telecommunication applications [27, 37].

2 Methods

2.1 Molecular Beam Epitaxy

This work mainly relied on the MBE equipment that was used to grow all of the semiconductor structures. A *Veeco GENxplor R&D MBE* system was used. The main principle of this technique is depositing materials coming from atomic or molecular "beams" onto a substrate where they form bonds and contribute to the growth of the layers. MBE is one of the most precise methods in semiconductor growth allowing sub-nanometer precision and highest interface quality in III-V semiconductor heterostructure growth. The high quality is ensured by ultra-pure source elements. In this work 7N5 purity Ga, As, Si and Be were used, while Bi and Al had a purity of 6N5. The source elements are housed in Knudsen cells (k-cells). The material flux coming out of the cells is controlled by the source temperature and pneumatic shutters. A special source design was used for As. To achieve a better sticking coefficient As_2 species were used, that were obtained by cracking the As_4 tetramers at elevated temperature of 900°C (more than two times hotter than the source bulk temperature). Since As is a highly volatile material, to ensure better flux control, the source has an additional diaphragm valve giving the ability to finely tune the flux ratios. A retractable ion-gauge was used to measure the material fluxes in BEP just below the substrate. To ensure a sufficient mean free path for the material flux and to limit impurity incorporation, growth is performed in ultra-high vacuum. The vacuum is maintained by a system of rotary, turbomolecular, cryogenic, and ion pumps, together with liquid-nitrogen cryopanels on the reactor walls. This allows the system to reach a typical idle pressure on the order of 10^{-10} Torr. During operation, the background pressure is commonly on the order of 10^{-7} Torr.

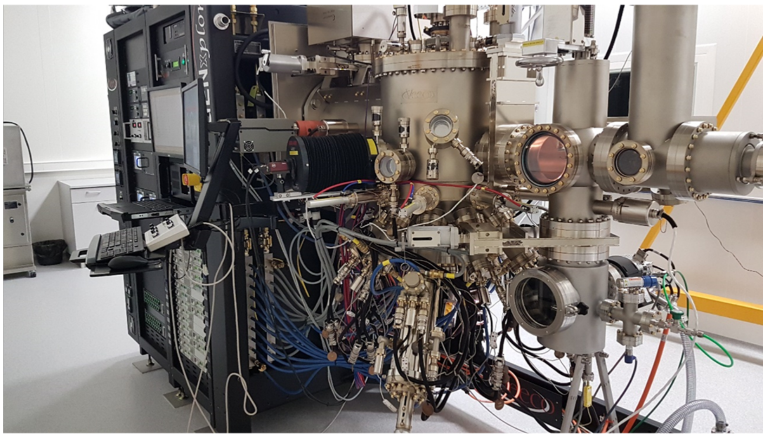

Fig. 10. Veeco GENxplor MBE system, (State Research Institute Center for Physical Sciences and Technology, Vilnius, Lithuania).

2.1.1 Temperature Control and Monitoring

Substrate temperature is one of the most crucial parameters in III-V semiconductor growth. The temperature is set by inputting a thermocouple setpoint that is connected in a feedback loop with the substrate heater. Since the thermocouple sets the heater temperature, the actual substrate temperature may vary, depending on the GaAs substrate conductivity, and thickness. Therefore, the temperature is additionally monitored using a "BandiT" band edge thermometer. This thermometry system works by measuring the transmission through the substrate, where the heater acts as an infrared light source. Given that semiconductor materials follow the *Varshni* relation of band gap versus temperature [38], by detecting the absorption edge of the transmitted spectrum the computer software estimates the temperature of the semiconductor wafer by comparing the shift in the absorption edge. This technique eliminates the geometry and substrate type ambiguities in the growth temperature, allowing for more precise control. This is crucial in ensuring reproducibility of GaAsBi-based structures.

2.1.2 In-situ Growth Monitoring

In-situ growth monitoring can give vital information about the composition and quality of the grown layers. Such monitoring is enabled by reflection high energy electron diffraction (RHEED), which operates on the basis of electrons from an electron gun grazing the substrate surface at a small angle (<3°). The electrons are diffracted from the surface, and the diffraction pattern depends on the surface reconstruction. The diffracted electrons hit a phosphor screen that is placed in front of a CCD camera. The pattern recorded by the camera can be interpreted in several ways. For the growth of GaAs the quality of the alloy can be estimated. If the substrate temperature is sufficient and the flux ratio is well calibrated a (2x4) RHEED pattern is observed, while (1x3) pattern is usual for LTG GaAs. When considering GaAsBi, RHEED provides a way to confirm the formation of the alloy during growth as signaled by (2x1) pattern. The reconstructions for LTG GaAs and GaAsBi are summarized in Fig. 11 [39].

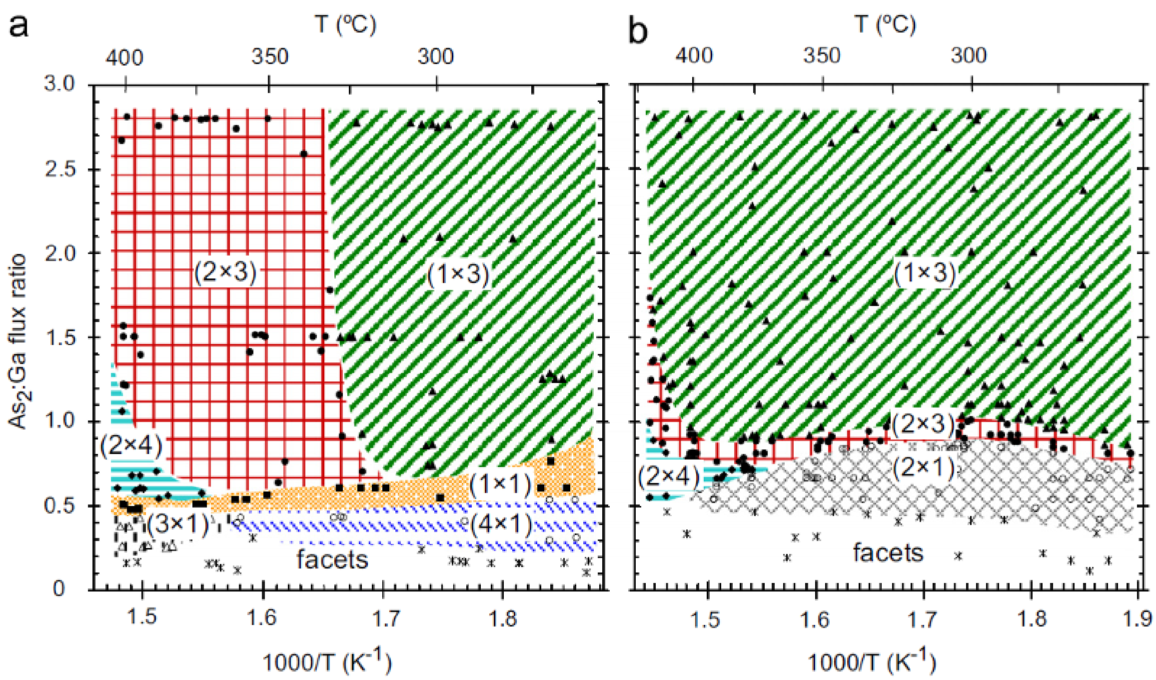

Fig. 11. RHEED patterns for a) LTG GaAs and b) GaAsBi at different As to Ga flux ratios and substrate temperatures. (2x1) pattern is attributed to GaAsBi, while (2x3) pattern in part b) is likely a mixture of (2x1) and (1x3). All other reconstructions are attributed to GaAs. Taken from [39].

Information can also be extracted from the RHEED intensity. Generally high intensity of the signal is attributed to high level of flatness. This is particularly useful in estimating the growth rate. When tracking the intensity evolution in time of the main reflection, it resembles a sine wave, this is caused by the growth of the material. At the initial point, the surface is flat, as growth is started islands start to form, decreasing the intensity of the diffracted light detected by the CCD. Since in MBE the usual growth is monolayer by monolayer, as the first monolayer is filled the intensity recovers to the maximum. From the time between two maxima, we can extract the duration of the growth of a single monolayer, giving the growth rate in ML/s. Furthermore, the decrease in RHEED intensity and disappearance of clear reconstruction provide the confirmation of sufficient Bi surface wetting layer, which is crucial for the growth of GaAsBi heterostructures as discussed in subsection 1.2.2.

2.2 Photoluminescence and Electroluminescence

PL and EL are powerful methods for investigation of emitter-focused structures. In this work PL was used to investigate the optical properties of GaAsBi QW calibration structures and for the extended investigation into growth regimes of GaAsBi layers. As PL provides a usually non-destructive way to probe the transitions in the semiconductors, all structures were characterized by PL to investigate the emission wavelength that closely corresponds to the band gap of grown structures. Spectral width was observed to evaluate the homogeneity of the epilayers. In addition, the PL intensity was used as a way to compare the quality of the structures, since a more defective structure would have lower emission intensity. The comparison of intensities between samples was enabled by a constant PL set-up, where the only changeable part is the sample itself. This set up was used for all RT measurements, where a diode-pumped solid-state laser (532 nm) was used to excite the samples with an intensity of 9 kW/cm^2. The PL from the sample was split using a grating monochromator and detected using lock-in amplification with an InGaAs detector. For temperature-dependent (TD) PL measurements the sample was housed in a closed cycle liquid He cooled cryostat enabling measurement in a range from 4 K to 300 K. For TD measurements a lower excitation intensity of around 12 W/cm^2 was used. It must be noted that in contrast to the RT set-up, the TD PL set-up was refocused for each sample making the intensities of TD PL spectra incomparable.

The same two detection systems were used to obtain RT and TD EL and lasing spectra. Current injection into LEDs was performed using a CW DC power supply (*Agilent U8002A*), while LDs were pumped with a high-voltage pulse generator (*AVTECH AVRZ-5W-B*) operating at a repetition rate of 1 kHz with a pulse duration of 50 ns. Output power of lasers was measured with a Ge-based photo detector (*Thorlabs PDA50B-EC*).

2.3 Absorption Measurements

Absorption spectra of the samples were measured using a grating monochromator (Leningrad Optical Mechanical Association MDP-23). The light coming from a lamp passes through a monochromator, being chopped at a moderate frequency and focused onto the sample surface, while the spectrum signal is measured by the Thorlabs PDA50B-EC Germanium Amplified Photodetector.

2.4 THz Spectroscopy

THz excitation spectroscopy was used to evaluate the direct band gap of the investigated samples. The measurements were performed using a THz time-domain spectroscopy system in which the sample itself acted as the THz emitter. The setup was driven by a Yb:KGW Light Conversion PHAROS laser operating at $\lambda = 1030$ nm, with a pulse duration of $\tau_p = 160$ fs and a repetition rate of $f = 200$ kHz. The generated THz radiation was detected using a GaAsBi photoconductive antenna (Teravil Ltd.).

For optical excitation of the samples, femtosecond pulses with wavelengths tunable from 1040 to 2600 nm were provided by a Light Conversion ORPHEUS optical parametric amplifier. The GaAsBi layers were excited in reflection geometry using a p-polarized beam with a 2 mm FWHM diameter and 60 mW average power. The beam was incident at an angle of 45° with respect to the sample surface normal. The obtained spectra show the peak-to-peak amplitude of the emitted THz pulse as a function of excitation photon energy, with the signal normalized to the same number of incident photons.

2.5 Structural and Surface Characterization

Rocking-curve and reciprocal-space-map measurements were carried out using a Rigaku SmartLab high-resolution X-ray diffraction (HRXRD) system in order to determine the thickness, Bi content, and strain state of the grown layers. The experimental data were analysed using GlobalFit software, with the lattice constants of GaAs and GaBi taken as 5.653 Å and 6.324 Å, respectively.

The layer thickness was also estimated from cross-sectional scanning electron microscope (SEM) images acquired using a Helios NanoLab 650 system. The same system was equipped with an INCAEnergy X-ray spectrometer from Oxford Instruments with an X-Max detector, which was used for energy dispersive X-ray spectroscopy (EDX) analysis of the droplet material composition. Surface SEM images were additionally used to assess the sample morphology and to extract droplet statistics.

Atomic force microscopy (AFM) measurements were performed under ambient conditions at room temperature using a Veeco Dimension 3100 scanning probe microscopy (SPM) equipment operated in tapping mode. Silicon cantilevers were used for the measurements (Bruker NCHV, $f_0 \approx 320$ kHz, $k \approx 40$ N/m, tip radius ≈ 8 nm).

3 Results & Discussion

In this section the main results obtained in this work will be presented and discussed. The chapter is split into three main parts. The section begins with a brief description of growth conditions that are general for all epitaxial structures presented in this work. Secondly, an in-depth investigation into the growth regimes of GaAsBi will be presented by investigating thick layers (nominal thickness of 115 nm). Lastly, the growth regime that is promising for the growth of quantum structures will be applied for GaAsBi-based LDs and LEDs.

3.1 Sample Growth

All samples were grown on (100) epi-ready GaAs substrates. For GaAsBi thick layers and QW calibration samples, semi-insulating 450 μm-thick substrates were used. Si-doped n-type (2×10^{18} cm^{-3}) and Zn-doped p-type (1×10^{19} cm^{-3}) substrates with a thickness of 350 μm were used for the growth of diode structures. All substrates were degassed prior to growth. Firstly, the sample is heated to 200 °C in the load-lock after which the initial degassing is continued at 300 °C in the buffer chamber. The first two stages are mainly used to outgas the weakly absorbed species that are mainly introduced into the holder and chamber during loading. The final preparation step happens just prior to the growth as the substrate is heated to around 650 ° C in As overpressure to remove the native GaAs oxides. The supply of As during this step is crucial as it prevents As desorption that is initiated at approximately 400 °C. Finally, all of the substrates were buffered by GaAs to achieve optimal surface flatness.

3.2 Growth of GaAsBi Layers

The growth of GaAsBi layers was used to clarify the growth window of the alloy. In this part, layers with a nominal thickness of 115 nm were grown at substrate temperatures ranging from 340 °C to 380 °C. The main technological parameters varied in this study were the As/Ga and Bi/Ga flux ratios. In MBE, the elemental fluxes are typically not measured directly as atomic fluxes, but are instead estimated from the BEP measured by an ion gauge positioned close to the substrate. However, BEP values are equipment dependent, since they are influenced by the geometry of the MBE system, ion-gauge sensitivity, source configuration, and the molecular species used. Therefore, the measured BEPR does not directly correspond to the true atomic flux ratio, but can be converted using an empirically determined calibration factor.

Up to this point, it has been widely accepted that good-quality GaAsBi is grown close to stoichiometric As/Ga conditions, corresponding to an atomic As/Ga flux ratio of approximately unity. In conventional GaAs MBE, the stoichiometric point can often be identified from a change in surface reconstruction, where the surface becomes Ga-terminated after the As flux is reduced below a critical value. However, this method is less suitable for low-temperature growth, since the reconstruction transition from As-rich (2×4) to Ga-rich (4×2) is typically observed only at higher growth temperatures. Furthermore, the stoichiometric point determined in this way is temperature dependent, because As desorption depends strongly on substrate temperature.

For this reason, alternative methods are required when calibrating the As/Ga ratio for GaAsBi growth. In this work, the stoichiometric point was determined by monitoring the grown-layer thickness and surface morphology. When As becomes the limiting species, the growth rate decreases and excess Ga accumulates on the surface in the form of droplets [40]. Using this approach, it was determined that, in our MBE system and within the investigated temperature range, the relationship between the measured BEPR and the atomic As/Ga flux ratio is approximately

$$\frac{\Phi_{\mathrm{As}}}{\Phi_{\mathrm{Ga}}} \approx \frac{\mathrm{BEPR}_{\mathrm{As/Ga}}}{4.4},$$

where Φ_{As} and Φ_{Ga} are the effective atomic fluxes of As and Ga, respectively. Thus, an atomic As/Ga flux ratio of unity corresponds to an As to Ga BEPR of approximately 4.4 in this system.

With this in mind, we start with the commonly referred optimal growth conditions around the BEP As/Ga of 4.4 and extend the window to cover a range of BEPR from 1 to 8. The total number of samples in the set is 30. For easier reading they are split into 4 series and named according to the BEP As/Ga and Bi/Ga used. For easier comparison of BEP Bi/Ga a reference value of 0.48 was taken as 100 % and others are recalculated accordingly. The naming convention is as follows: series I corresponds to BEP As/Ga $\leq$ 2, series II to $2 < \mathrm{BEP\,As/Ga} \leq 3.5$, series III to $3.5 < \mathrm{BEP\,As/Ga} \leq 5$, and series IV to BEP As/Ga $>$ 5. Due to the larger number of samples within series III, this series is further subdivided according to the Bi flux. For clarity, samples are labeled as III-L (BEP Bi < 80%), III-O (80% $\leq$ BEP Bi $\leq$ 120%), and III-H (BEP Bi > 120%). L stands for low, H for high, and O for original. The main technological parameters are summarized in table 1.

3.2.1 GaAs Growth with Bi Surfactant

First, we investigate the samples in the series IV. Here the BEP As/Ga is between 6.25 and 8.11, corresponding to a flux ratio of around 1.4 to 1.85. In this range the Bi incorporation is not expected as As out-competes Bi for the lattice sites. However, Bi flux was still supplied because Bi tends to remain at the growth surface as a surfactant. It modifies the surface energy and enhances adatom redistribution before incorporation, thereby smoothing terraces and improving interface planarity [22, 41, 42].

The structures were investigated using RT PL. All of the samples in series IV exhibited a sharp PL peak at around 1.42 eV, corresponding to emission from pure GaAs. This signifies that Bi is not incorporated at such conditions. The only sample that had a PL signal at lower energy was IV-2 (see Fig. 12). While this peak could signal possible Bi incorporation, we suppose that this is caused by LTG GaAs defects rather than GaAsBi emission. This sample was grown at low temperature of 345 °C and a BEP As/Ga of 6.25. Since good quality GaAs is grown at much higher temperature and at a large As overpressure, the growth conditions are likely to cause high density of defects. The hypothesis is further backed-up by HRXRD rocking curve scans, which do not show any Bi related features. Furthermore, the width of the peak is quite large, a FWHM is more than 220 meV, far from the approximately 100 meV usual for GaAsBi emission.

Table 1. Summary of the technological growth parameters used for the samples presented in this work. Horizontal lines separate the different sample series. The T_{growth} refers to the substrate temperature measured using BandiT. As/Ga and Bi/Ga denote the BEP ratios measured prior to growth for the As, Ga, and Bi sources. The BEP Bi% value is a calculated parameter derived from BEP Bi/Ga, where a value of 0.48 is taken as the reference corresponding to 100%.

Sample	T_{growth} (°C)	BEP As/Ga	BEP Bi/Ga	BEP Bi(10^{-7} Torr)	BEP Bi (%)
I-1	364	1.01	0.74	1.55	153
I-2	375	1.26	0.82	1.48	169
I-3	377	1.44	0.42	0.76	86
I-4	360	1.91	0.51	0.90	104
II-1	354	2.79	0.54	0.86	112
II-2	363	3.11	0.54	0.86	112
III-O1	339	3.69	0.53	0.87	110
III-O2	335	3.73	0.51	0.90	104
III-O3	336	4.41	0.48	0.78	100
III-O4	353	4.47	0.53	0.87	110
III-O5	354	4.48	0.43	0.69	89
III-O6	352	4.54	0.54	0.87	112
III-O7	352	4.54	0.48	0.78	100
III-O8	351	4.65	0.48	0.78	100
III-O9	583	4.90	0.53	0.87	109
III-O10	353	4.90	0.53	0.87	109
III-L1	352	4.10	0.37	0.60	77
III-L2	350	4.48	0.25	0.40	51
III-H2	349	4.44	0.63	1.01	132
III-H1	352	4.44	0.71	1.13	147
IV-1	583	6.25	0.52	0.87	108
IV-2	345	6.25	0.52	0.87	108
IV-3	580	8.10	—	—	
IV-4	359	8.10	—	—	
IV-5	580	8.11	0.55	0.92	114
IV-6	337	8.11	0.55	0.92	114

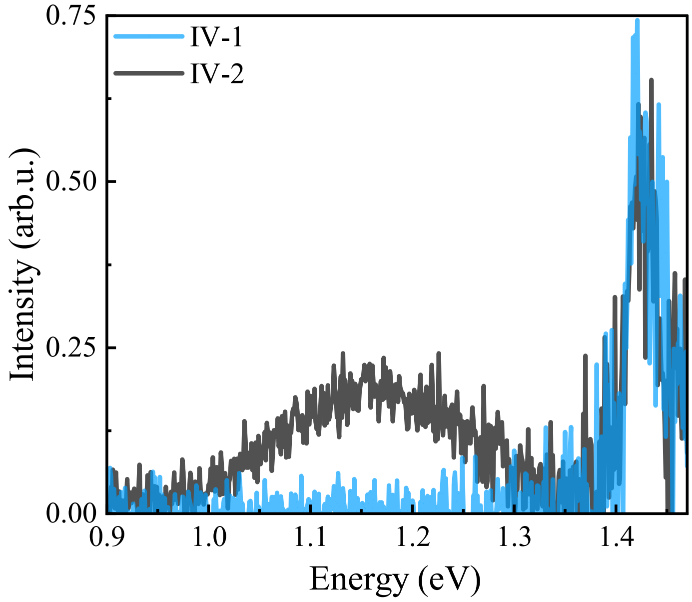

Fig. 12. RT PL spectra of samples from series IV grown using BEP As/Ga - 6.25. Blue line - sample IV-1 grown at 583 °C; Black line - sample IV-2 grown at 345 °C.

The surface of all samples was very smooth except for a few loop-type dislocations originating from the GaAs substrate, that can be seen in large scale differential interference contrast (DIC) picture in Fig. 13. AFM mapping of the samples also proved the good surface roughness even for the samples grown at low temperature. Sample IV-2 had a roughness Sa = 0.15 nm, which is considered to be smooth for GaAs, equating to approximately half of a GaAs monolayer thickness of 0.28 nm (see Fig. 13).

All in all, the results obtained from the samples of series IV, show that the incorporation of Bi is completely suppressed when operating at BEP As/Ga > 6.25, as signified by X-ray diffraction (XRD) and PL signal that is attributed to emission from GaAs. On the other hand, it was shown that the use of Bi as a surfactant can be used to achieve low roughness of GaAs surface even at low temperatures.

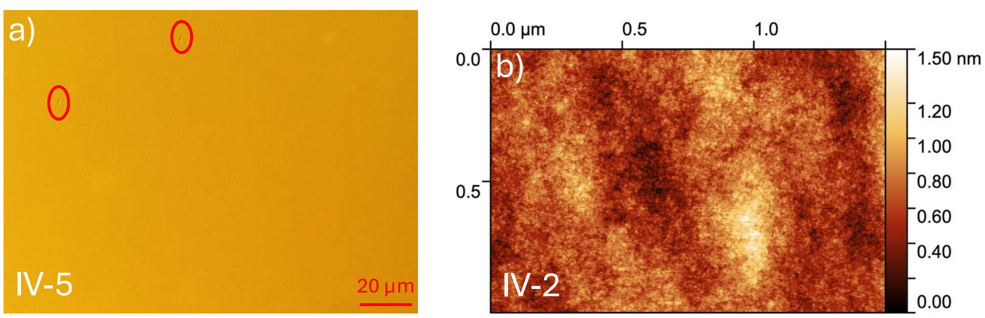

Fig. 13. Surface morphology of samples from series IV. a) DIC image of sample IV-5 (BEP As/Ga - 8.11, growth temperature 580 °C), defects originating from the substrate circled in red; b) AFM map of sample IV-2 (BEP As/Ga - 6.25, growth temperature 345 °C), the roughness of the sample was Sa = 0.15 nm and Sq = 0.19 nm.

3.2.2 Stoichiometric growth of GaAsBi

For this series (III), the classical growth window of atomic flux close to unity (0.84 to 1.11 in this series) was used. Most samples in this series were grown under similar temperature and BEP As/Ga conditions. A large variation in Bi flux was used, in addition to several samples being grown at lower temperature, to investigate the limits of Bi incorporation in the temperature-limited growth regime (discussed in subsection 1.2). For samples grown at substrate temperature of 350 °C and Bi flux in the range of 89 % to 112 %, good reproducibility was achieved with emission energy in the range of 1.05 eV to 1.11 eV. Generally, the samples exhibited comparably intense PL signal with a typical FWHM of around 100 meV. When contrasting the spectral features of sample IV-2 (see Fig. 12 in section 3.2.1) with samples in series III, we see a large narrowing of the PL peak, reduction in noise, increased intensity, and the absence of GaAs emission lines (see Fig. 14). The contrast in these results allows to confirm that in these growth conditions emission from GaAsBi is achieved, moreover it is done reproducibly, as illustrated by samples III-O4 and III-O6, which were grown at almost identical growth conditions to prove the reproducibility.

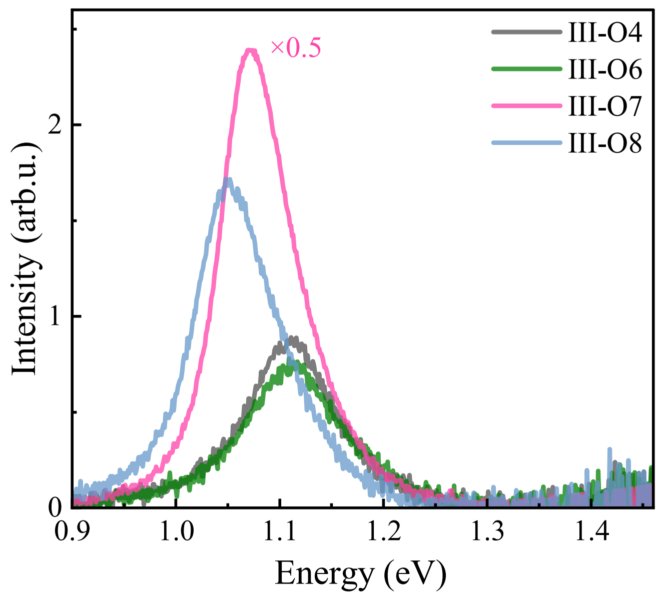

Fig. 14. RT PL spectra of samples from series III-O grown using BEP As/Ga - 4.47 to 4.65 and substrate temperature of ≈ 352 °C. The intensity of sample III-O7 (pink) is divided in half for easier comparison.

Moreover HRXRD rocking curve and reciprocal space mapping (RSM) measurements reinforce PL results. For the sample III-O4 the rocking curve scan shows a Bi content of 4.15 % and a thickness of 111 nm (4 nm deviation from the nominal thickness) (see Fig. 15). Additionally, the scan shows sharp periodic fringes, and a well pronounced GaAsBi peak, hinting at the high crystalline quality, sharp GaAs/GaAsBi interface, and high homogeneity of Bi distribution. RSM of sample III-O7 (4.65 %Bi) shows that there is no sign of relaxation in the grown layers, supporting the advantage of GaAsBi in managing strain discussed in subsection 1.1. The Bi contents estimated by HRXRD are consistent with the emission energies obtained from PL, giving an approximate band-gap reduction of 75 meV/%Bi. In this calibration, 4.15 %Bi corresponds to a peak position of 1.11 eV, while 4.65 %Bi corresponds to 1.07 eV. Such values are consistent with publications by other groups.

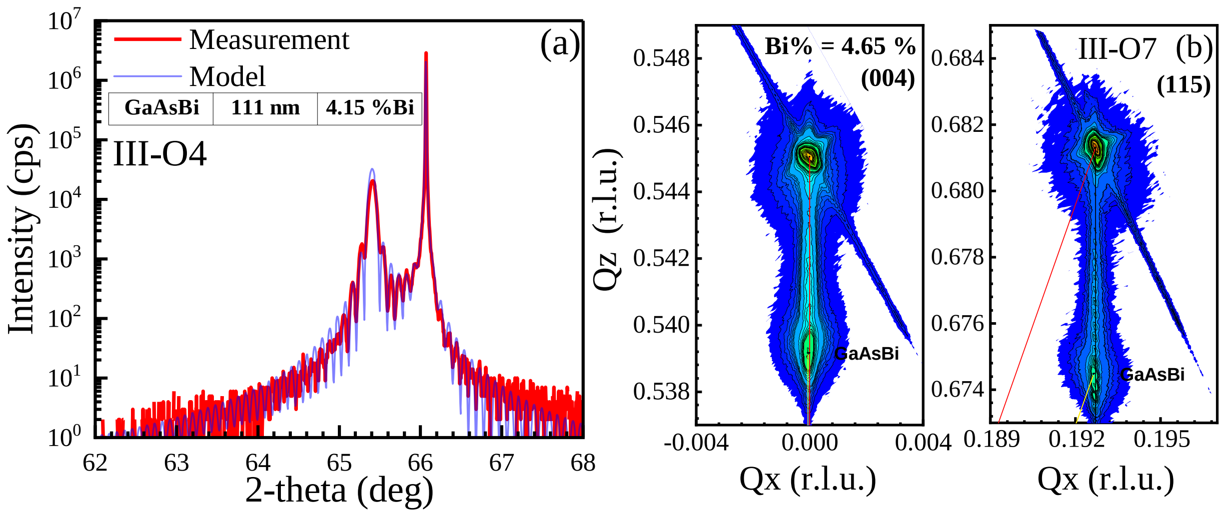

Fig. 15. a) XRD rocking curve scan of sample III-O4, b) RSMs of sample III-O7 are shown for the (004) and (115) planes.

Furthermore, we investigate the effects of Bi flux and temperature. The good reproducibility of the emission energy in a narrow Bi flux range of 89 % to 112 %, suggests that the growth is in fact temperature limited. To test the limitations of this growth regime the Bi flux was varied drastically from as low as 51 % to 147 %.

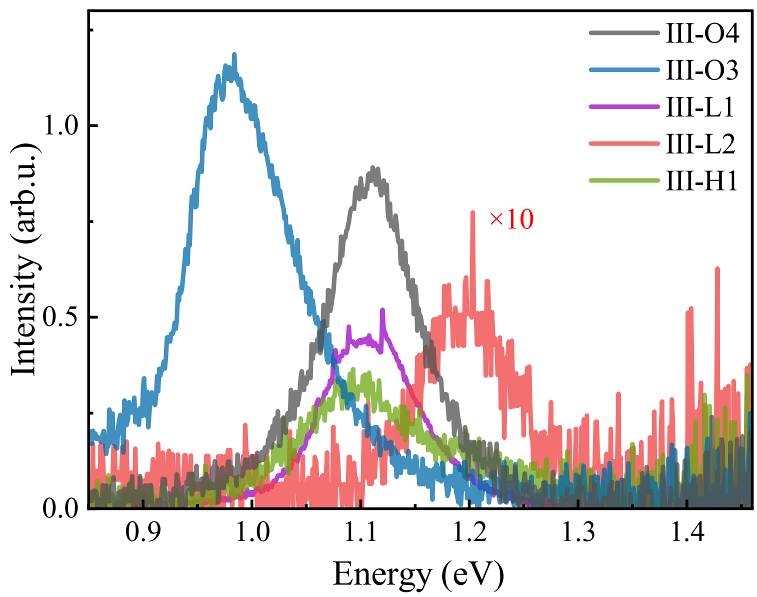

Fig. 16. Comparison of RT PL spectra of samples from series III-O, III-L, and III-H. A red-shift for sample III-O3 is observed due to a lower growth temperature (336 °C). Decreased intensity due to sub-optimal Bi flux is seen for samples III-H1 III-L1, and III-L2 (multiplied 10 times for clarity).

Additionally, sample III-O3 was grown at 20 °C lower temperature, to prove the possibility of controlling the emission energy, solely by the substrate temperature for GaAsBi layers. The trends observed by acquiring PL spectra are summarized in Fig. 16.

Lowering the growth temperature provides a straightforward result. The sample grown at 336 °C exhibits a red-shifted PL signal by about 100 meV, peaking at 0.98 eV, proving the temperature-limited condition window. The influence of Bi flux can be interpreted by taking the sample III-O4 as reference. It is seen that we can extend the temperature-limited window down to Bi flux of 77 %. Furthermore, by increasing the Bi flux to 147 % no shift in emission energy is observed. A further decrease in Bi flux down to 51 % resulted in a large shift of emission wavelength, with the PL signal peaking at 1.2 eV. The fact that Bi flux becomes the limiting condition for incorporation is supported by HRXRD, where the estimated Bi fraction is 2.6 %.

These trends match the ones seen by surface investigations. As interpreted from the surface feature shape and EDX mappings, the surface agglomerates in the discussed growth condition window are usually pure Bi clusters (see Fig. 17). By decreasing the Bi flux for the sample III-L2, the surface generally improved, and the Bi droplet size decreased drastically. Contrasting this with the other two samples presented, it can be concluded that the reduction of Bi flux resulted in less accumulation of Bi on the sample surface, because most incoming Bi atoms are incorporated into the lattice sites.

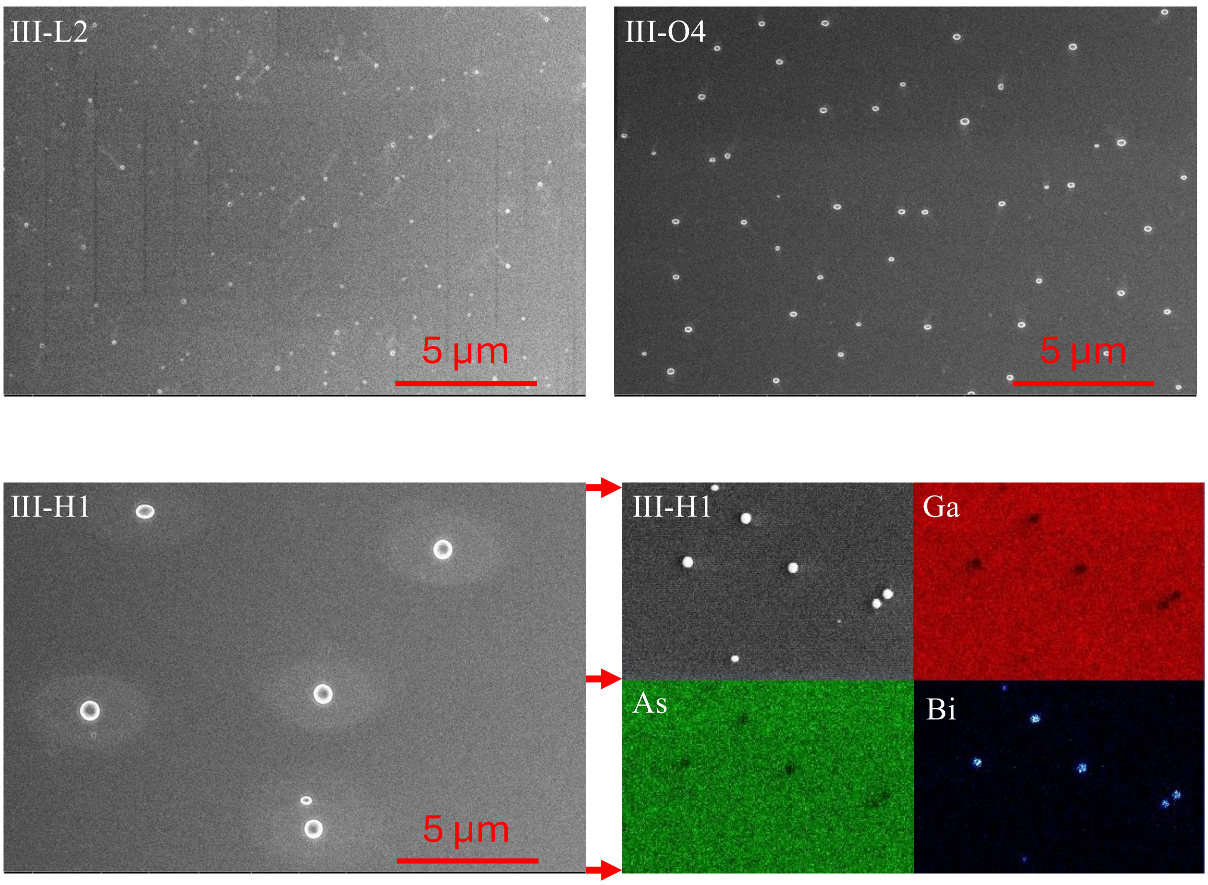

Fig. 17. Typical SEM surface micrographs for samples from the series III, an EDX image (Ga - red, As - green, Bi - blue) of sample III-H1 confirms the presence of pure Bi droplets on the surface.

Despite the increased surface quality of sample III-L2, the general trend for all samples in series III is the high sensitivity of PL intensity to Bi flux. Deviations away from the optimal value (100 % in this case) result in a sharp drop in emission intensity (see Fig. 18), while only a drastic change in the Bi flux could be used to control the emission energy as illustrated by the sample III-L2 (see Fig. 16).

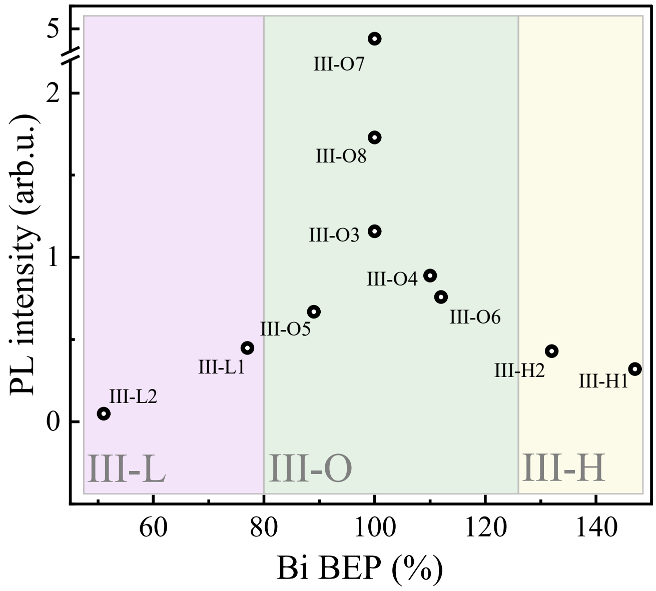

Fig. 18. PL peak intensity dependence on Bi flux of samples grown in the BEP As/Ga range of 4.10 to 4.65. Colored background serves as eye-guide for separation of sub-groups in series III. III-L - magenta; III-O - green, III-H - yellow.

To conclude this subsection, it can be stated that the growth conditions used for series III are suitable for the growth of thick GaAsBi layers, showing ability to achieve intense PL signal with a moderate peak width. Nevertheless, this growth window has a very high sensitivity to Bi flux, and requires extensive calibration to achieve an optimal result.

3.2.3 As-Limited Growth of GaAsBi

Series II consisted of two samples grown at slightly As-limited conditions. The main purpose of this series was to investigate the changes in samples grown at conditions that are commonly referred to as sub-optimal. Here the Bi flux was kept constant mainly focusing on the influence of reduced As source pressure. The initial results show expected tendencies. While contrary to studies by *Richards et al.* and *Puustinen et al.* [6,7], the Bi incorporation was not suppressed, as the samples exhibit emission peaks at 1.07 to 1.11 eV shown in Fig. 19 (the shift attributed to the change in substrate temperature). Nonetheless, there is a strong influence on the emission intensity. It is seen in Fig. 19 that the spectra are low intensity, noisy, and have a wider spectral shape. Moreover, these conditions cause surface roughening, with a large surface coverage by biphasic Ga-Bi droplets (see Fig. 21). The appearance of unincorporated Ga shows that the effective growth rate is decreased, as the growth rate becomes fully governed by the As supply.

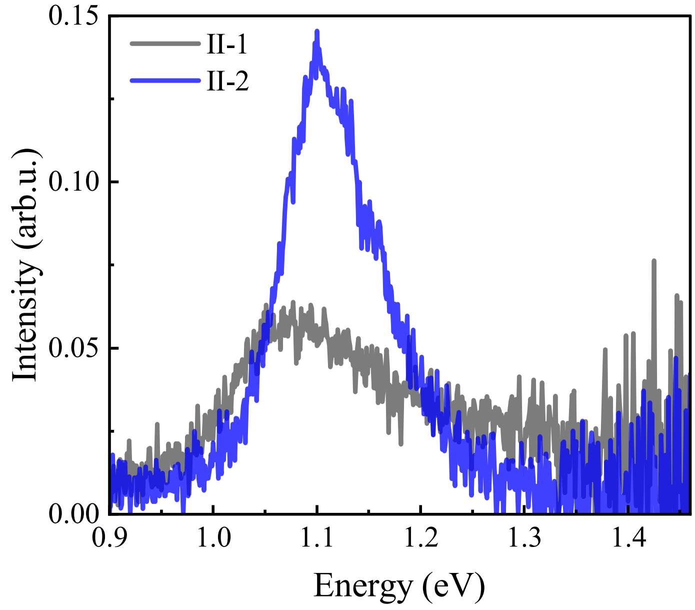

Fig. 19. RT PL spectra of samples II-1, and II-2, illustrating a decrease in optical properties.

The HRXRD measurements confirm the Bi incorporation to be at around 4% Bi content in both samples, by the clear peak originating from GaAsBi. On the other hand, HRXRD could not be used to evaluate the layer thickness, as the rocking curve scans were free of any fringes (see Fig. 20). This absence of fringes also shows that the crystalline quality of the sample is worsened. To prove the reduced thickness in comparison to the nominal, caused by group-V limited growth, cross-sectional SEM micrographs were acquired (see Fig. 21).

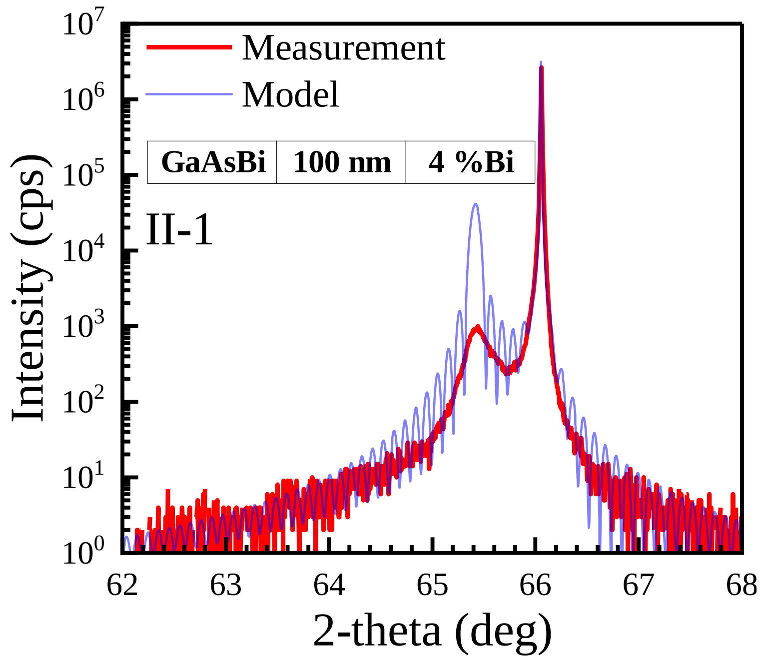

Fig. 20. XRD rocking curve scan of sample II-1. The thickness value given in the table was used to make the model. Due to the absence of fringes it does not represent the accurate layer thickness.

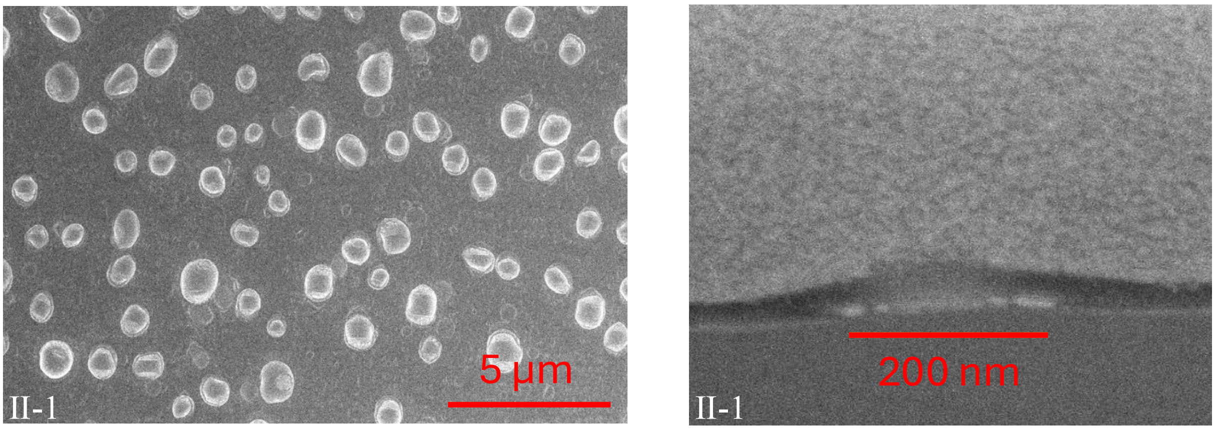

Fig. 21. SEM micrographs of sample II-1. The surface picture illustrates the large deterioration of surface quality (left). The cross-sectional image confirms that the thickness is lower than nominal (right). Moreover, the picture illustrates one of the periodically spaced pockets with Bi nanostructures.

The cross-sectional images revealed that the thickness is indeed lower than nominal, likely in the range of around 50 to 60 nm. The surprising result was the periodically spaced pockets containing high-contrast, bright, nm-scale features. Such features are attributed to Bi clusters. In earlier works it was shown that pure Bi clusters have the potential to produce quantum dot (QD) emission [43,44]. While SEM pictures are not sufficient to confirm the exact size and shape of these nanoparticles, this initial result shows promise for investigating this growth window further, for possible applications in 0D or 1D Bi nanostructures.

All in all, the results from series II confirm that it is possible to incorporate Bi into the GaAs lattice in As-limited conditions. Nonetheless, the use of such growth conditions results in worse optical and structural properties. The appearance of periodically spaced pockets with Bi nanoparticles shows promising features of such growth conditions for possible investigations into QD formation mechanisms.

3.2.4 The New High Quality GaAsBi Growth Window

Four samples are investigated in series I. In this section the focus was on further reducing the As flux (BEP As/Ga from 1 to 1.9). The limitation in As flux was clearly seen in both HRXRD and SEM measurements. For this series the thickness estimated from rocking curve scans varied between 30 and 50 nm. This decrease in thickness was further verified by SEM where the samples showed high surface area coverage of Ga or biphasic Ga-Bi droplets. Notably, compared to series II, the surface Ga fraction was heavily increased. This aligns with the large As limitation causing more unincorporated Ga to deposit in metallic form on the surface. The HRXRD and SEM trends are summarized in Fig. 22.

When considering the PL signal of these samples, a surprising result is observed as the spectral quality recovers from the series II samples. The emission energy of 1 to 1.1 eV is observed, and the emission intensity is considerably high.

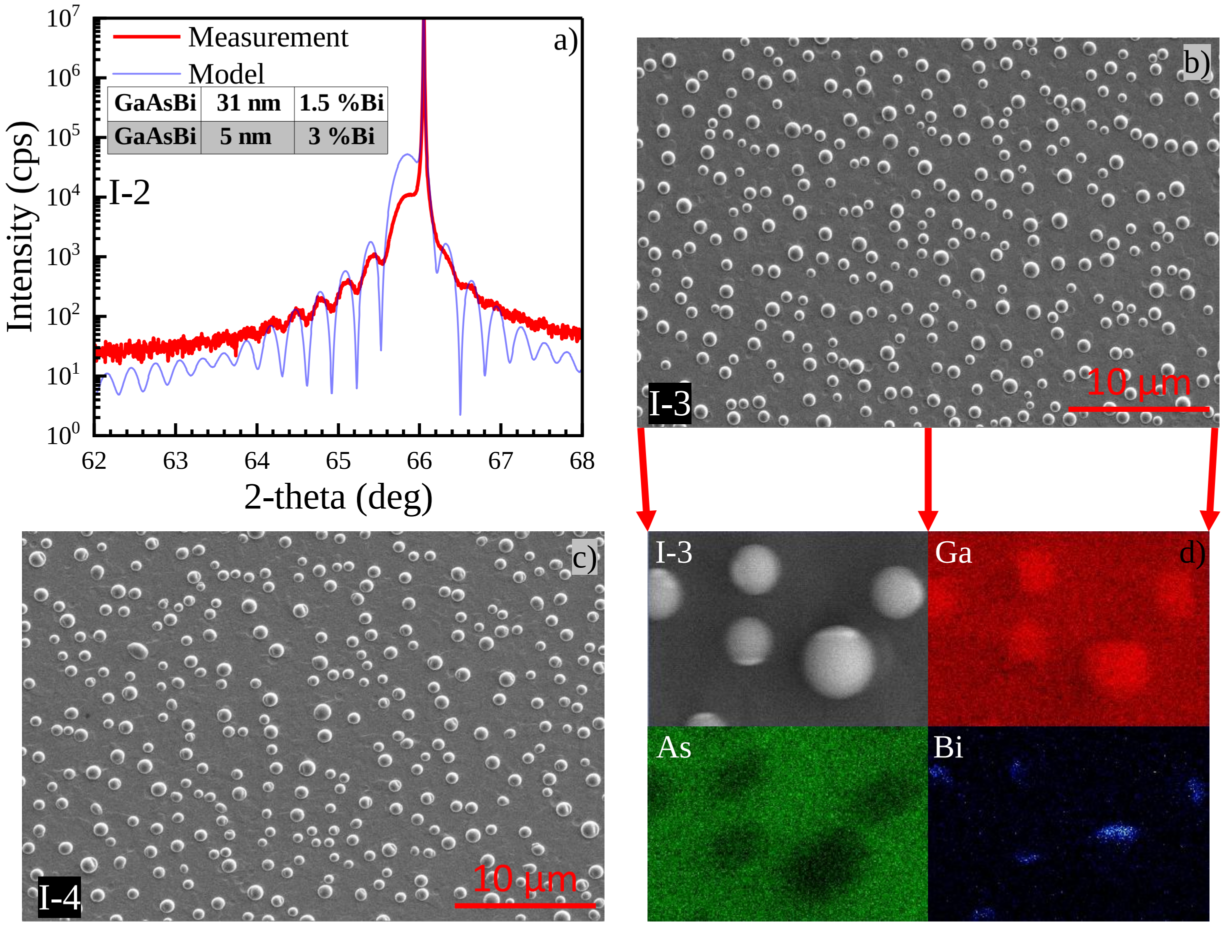

Fig. 22. a) XRD rocking curve scan of sample I-2. The table summarizes the parameters used to model the scan. b) and c) SEM micrographs of samples I-3 and I-4, respectively. d) EDX images (Ga - red, As - green, Bi - blue) of sample I-3, showing that Ga droplets dominate in the surface features.

Moreover, the emission linewidth is reduced, with FWHM values below 100 meV and as low as 86 meV for sample I-2 (see Fig. 23).

An ambiguity in this set of samples arises from the mismatch between the HRXRD and PL results. Initial modelling of the rocking-curve scans showed that these samples are far from the nominal thickness, which can be explained by the Ga accumulation seen under group-V-limited growth. The surprising result was the low Bi-content estimate, between 1 and 2.5 %. The emission energy obtained from PL, however, cannot be explained by such Bi contents. Based on the values obtained for series III, a Bi content of at least approximately 4 % would be required to produce emission near 1.1 eV. Consequently, one of the rocking-curve scans was remodeled under the assumption that two GaAsBi regions with different compositions are present (see Fig. 22 a). In this model, the low-Bi-content region represents the dominant part of the layer volume and therefore contributes most strongly to the HRXRD response, while a thinner region with higher Bi content accounts for the low-energy PL emission. It is supposed that the Bi-rich layer is grown initially, and the As-limited conditions allow to homogeneously incorporate a large amount of Bi. At the same time, Ga starts to accumulate on the surface.

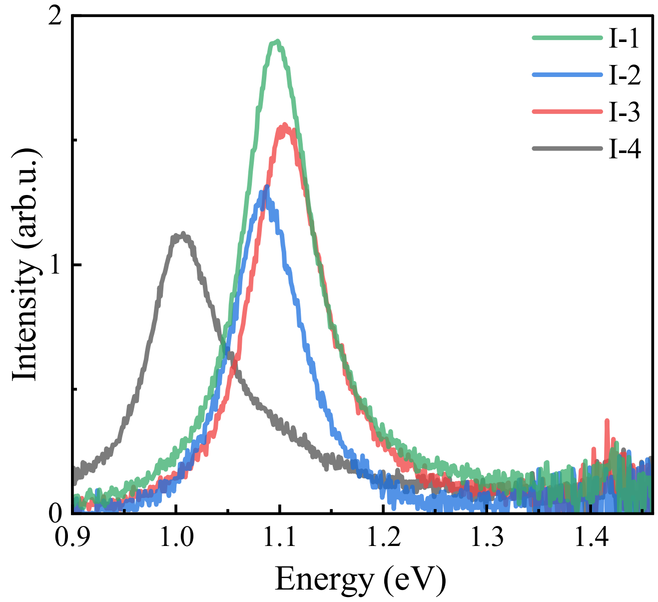

Fig. 23. RT PL spectra of all samples grown in series I. The increase in intensity and reduction in emission linewidth show the enhanced emission properties achieved in the As-limited growth regime.

Since the Bi incorporation mechanism proposed by *Lu et al.* [25], describes the incorporation into the lattice from a group-V terminated surface (discussed in subsection 1.2.2, see Fig. 8), it is likely that after a critical Ga accumulation the incorporation becomes suppressed, and the mechanism changes. While the absolute values shown in the Fig. 22 still do not match the emission, this serves as an example that the rocking curve scan can be modeled as double Bi content structure, which can be used to explain the disagreement between the two measurements.

All in all, in this subsection we described the growth of GaAsBi under extremely As-limited conditions. The PL spectra show promising features in terms of narrower peak width, and high emission intensity. While the conditions are not suitable for thick layer growth, they can be advantageous for thinner structures like MQWs.

3.2.5 Comparison of Optical Properties of GaAsBi Layers

In this subsection, optical properties of the samples will be compared further. As the PL from series IV showed no GaAsBi related emission, these samples are not considered in this comparison.

THz Excitation Spectroscopy and Absorption of GaAsBi Layers

First, additional spectroscopic methods were used to clarify whether the emission observed in the PL spectra originates from band-to-band transitions rather than defect-related recombination.

THz excitation spectroscopy was used to determine the direct band gap of the investigated samples. This method is well suited for semiconductor band-structure studies, since the generated THz signal is strongly related to the absorption of the excitation pulse and the subsequent ultrafast carrier dynamics [45].

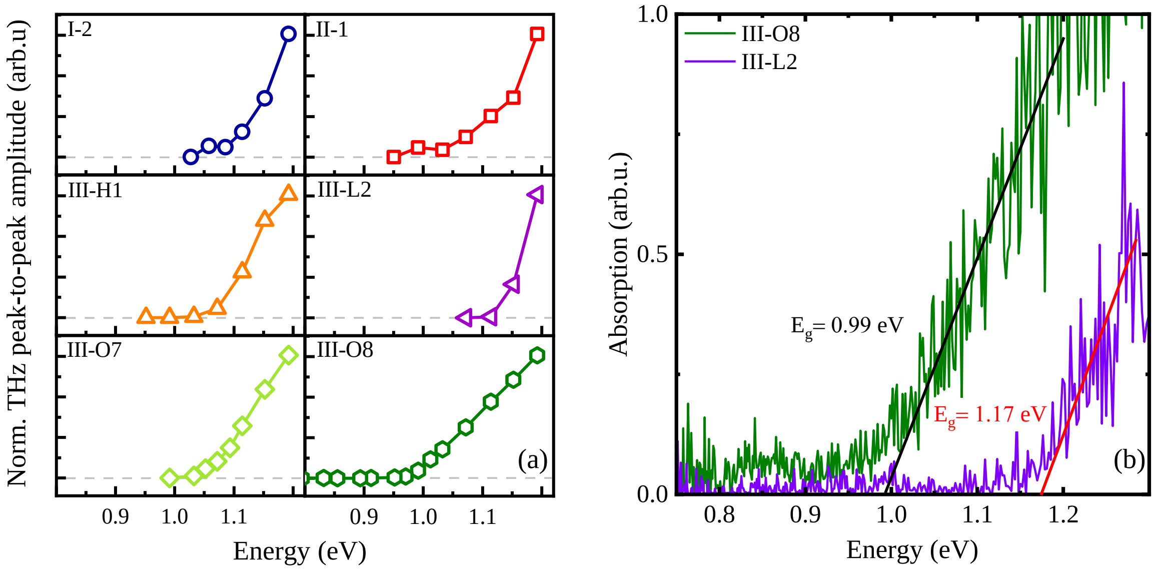

Fig. 24. (a) Normalized THz peak-to-peak amplitude as a function of excitation photon energy for samples I-2, II-1, III-H1, III-L2, III-O7, and III-O8. (b) Absorption measured in transmission geometry for samples III-O8 and III-L2. The blue and red lines are guides used to estimate the absorption edge of the respective samples.

The spectra presented in Fig. 24 show the dependence of the THz peak-to-peak amplitude on the excitation photon energy. For samples I-2, II-1, III-H1, III-L2, III-O7, and III-O8, a clear onset of the THz signal is observed, which is attributed to the absorption edge of the GaAsBi layers. Above this onset, the THz amplitude increases monotonically with excitation photon energy.

The emitted THz pulse is generated at the semiconductor surface by the rapid formation of a transient photocurrent after optical excitation. This current can originate from carrier drift in the surface electric field, or from the photo-Dember effect, where electrons and holes separate due to their different mobilities and form a rapidly changing dipole, similar to the mechanism observed in GaAs [46]. Therefore, the sharp increase in THz amplitude marks the onset of direct optical absorption. From these measurements, the direct band gap of the investigated GaAsBi layers was found to vary from approximately 0.98 eV to 1.14 eV, depending on the incorporated Bi content.

The absorption spectra of the samples were investigated in transmission geometry. The samples had an onset at around 1 to 1.2 eV correlating well with the PL spectra, XRD results, and growth conditions. The highest energy absorption onset was registered for the sample with lowest Bi content (see Fig. 24 b).

Together these measurements illustrate that the emission observed in PL spectra is related to the band-to-band transitions and that the spectra can be directly used for estimating the Bi content in the structures, clarifying the influence of growth conditions. More importantly, THz excitation spectrum of sample I-2 (see Fig. 24 a) shows that the direct band gap observed by this technique is at around 1.1 eV, which matches well with the PL spectra presented in Fig. 23 and helps to further clarify the ambiguity caused by HRXRD measurements discussed previously in subsection 3.2.4.

Temperature-Dependent Photoluminescence of GaAsBi Layers

TD PL spectroscopy was used to investigate the differences between the series, the measurements are presented in Fig. 25. For samples II-1 and III-H1, the trends observed previously are also present as the sample from series II had very low emission intensity, which prevented the measurement in the full temperature range. Both II-1 and III-H1 had noticeably broader emission bands compared with samples from series I and III-O. For sample III-H1 the FWHM at 4 K is 125 meV, increasing to 150 meV at 150 K, and recovering to 115 meV at 300 K. On the other hand, for III-O8 the FWHM at 4 K is only 105 meV, getting to 94 meV at 300 K, whereas series I exhibited the narrowest emission bands; for example, sample I-1 had a FWHM of only 64 meV at 4 K, increasing to 84 meV at 300 K.

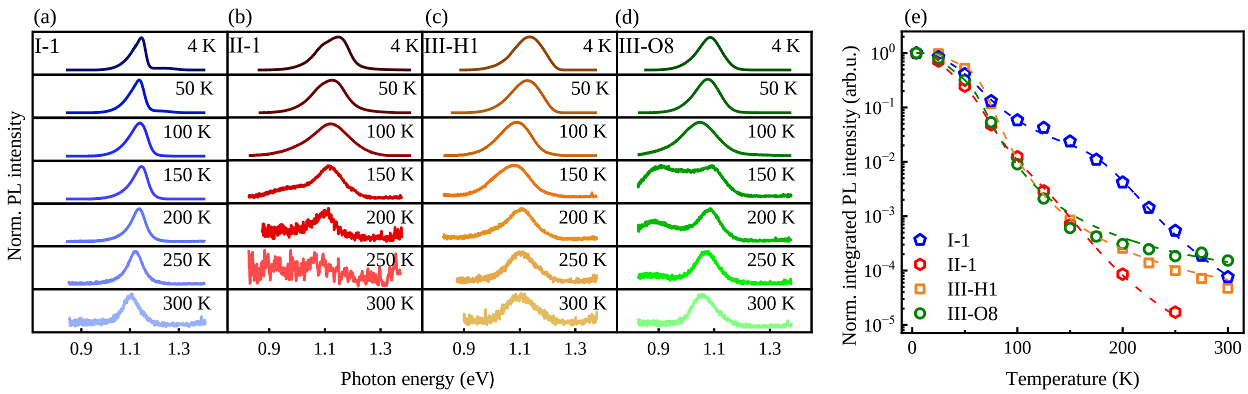

Fig. 25. TD PL of samples I-1 (a), II-2 (b), III-H1 (c), and III-O8 (d). Normalized intensity spectra measured from 4 K to 300 K in panels. The 300 K spectrum of sample II-1 (b) is not shown, as no signal was detected under the applied excitation power. (e) Corresponding normalized integrated PL intensity as a function of temperature.

When considering the PL intensity quenching with temperature we see another advantage of series I, as it has the lowest quenching out of all, especially visible in the temperature range of 75 K to 250 K, a range that could be applicable in device operation with moderate cooling. The series III and II have similar quenching behavior until the 150 K mark, from where the low quality of samples in series II results in the sample having the highest PL quenching out of all.

3.2.6 Comparison of Surface Morphology of GaAsBi Layers

In the wide range of growth conditions, many different surface features were observed characteristic of the technological parameters used. A comprehensive picture of the surface evolution at different BEP As/Ga, and Bi flux used is given in Fig. 26. Starting with the samples from series I, generally round shaped droplets are observed, as confirmed by EDX of sample I-3, they are almost fully Ga, corresponding to a highly group-V limited growth region. Meanwhile, in this growth condition window, the changes in Bi flux do not show substantial impact on the surface morphology. By increasing the BEP As/Ga irregularly shaped features are observed. The smooth, and round part of the features are Ga, while the crystallized irregularly shaped region is Bi, which is more prominent here, when comparing with samples in series I. This is caused by the increase in As flux resulting in more Ga incorporation, while having little influence on the amount of incorporated Bi, making the Bi part more prominent. For sample III-O2, where the BEP As/Ga is around 3.7 the Bi part in the features is further increased and a clear biphasic nature of the droplet is observed in the EDX pictures. Here the density of the features is smaller, but the size of the droplets becomes very random. Additionally, this sample had the largest droplet diameter. When approaching the optimal BEP As/Ga value of around 4.5, a shift in morphology is seen, as no more metallic Ga is seen on the surface, since all of it is incorporated into the semiconductor lattice (visible in EDX of III-H1 and III-O8 in Fig. 26). Here some sensitivity to Bi flux is observed, as the samples from series III-H have larger and denser Bi droplet population. This is explained by the fact that Bi incorporation was purely temperature-limited in this conditions range, resulting in the same Bi incorporation for all samples, while the excess Bi is observed accumulating on the surface. Finally, an uncharacteristically high density of droplets is seen for the sample III-O10, which can be attributed to the suppressed Bi incorporation due to the BEP As/Ga approaching to 5, resulting in metallic Bi on the surface, and not in the GaAsBi lattice.

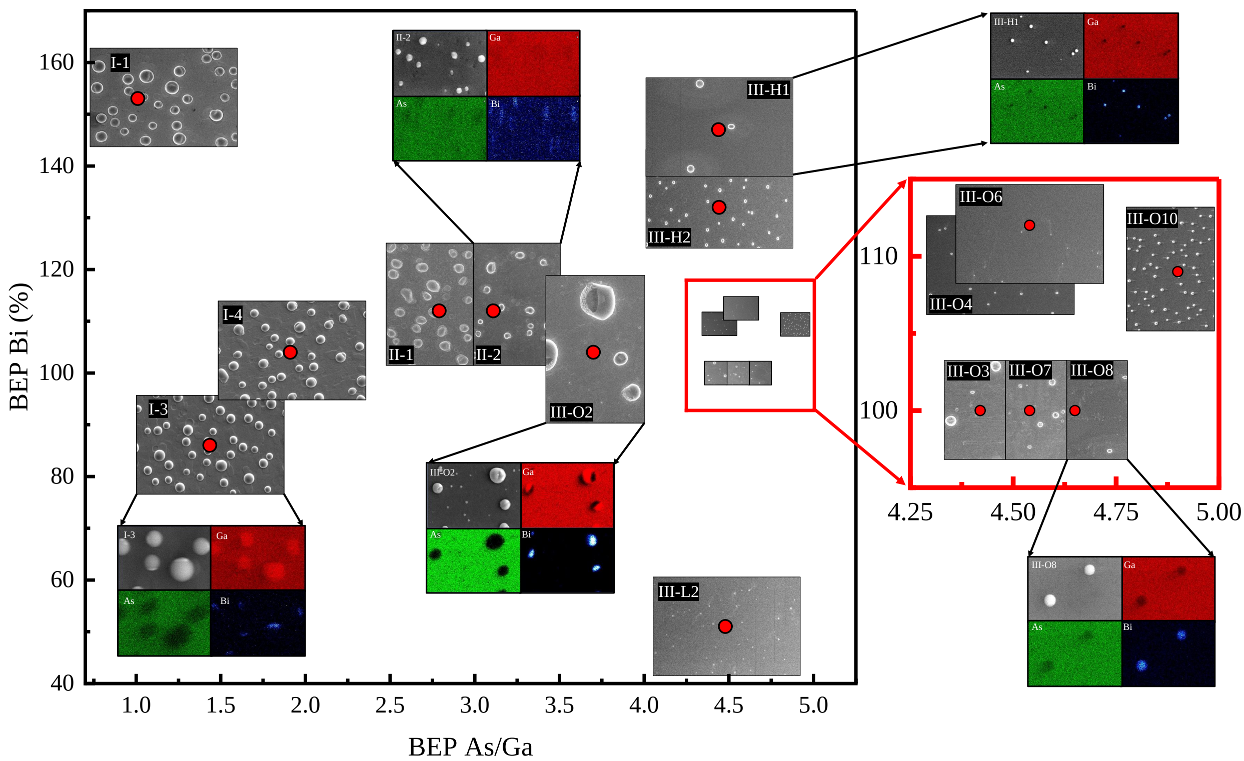

Fig. 26. SEM images of the analyzed samples, the scale is retained for all pictures making them directly comparable. The images are arranged according to their position in a BEP As/Ga versus BEP Bi space. In each SEM image, a red circle indicates the exact growth conditions corresponding to the sample. The red square in the diagram, spanning the region 4.25 < BEP As/Ga < 5 and BEP Bi between 95 and 115%, highlights the area that is enlarged for improved clarity. For samples I-3, II-2, III-O2, III-O8, and III-H1, corresponding EDX maps are presented, where elemental composition is shown by color: Ga (red), As (green), and Bi (blue).

Surface Droplet Statistics

To further clarify the relationship between growth conditions and surface quality, statistical analysis of the surface features was carried out. AFM and SEM image analyses were used to quantify the surface features formed during growth, particularly metallic droplets. For the SEM images, the detection procedure first isolated droplet footprints using a sequence of image-processing steps designed to suppress background variations and refine particle boundaries. The resulting masks were then filtered according to geometric parameters, such as size and circularity, so that only features consistent with droplets were retained for quantitative analysis. The main quantities extracted from the SEM images were the droplet diameter and the masked surface area. For elliptical droplets, the diameter was defined as the length of the major axis.

For AFM data, the detection procedure was more direct, since each pixel contains numerical height information rather than grayscale intensity. Droplets were therefore identified as regions with height values significantly above the surrounding background roughness. This allowed not only the lateral size of the droplets to be estimated, but also their volume. In addition, the droplet roundness was calculated as the ratio between the minor and major axes of an ellipse, with a value of 1 corresponding to a perfectly circular feature. In contrast, a value closer to 0 indicated decreased circularity.

First, the total surface area covered by metallic droplets was evaluated using SEM images, since these images cover a larger area and therefore provide more representative statistics. As shown in Figure 27(a), the droplet-covered surface fraction decreases with increasing As/Ga BEPR. For samples grown with As/Ga BEPR values of 4 or higher, the area covered by metallic droplets remains below 3%, and approaches 0% for samples grown close to Bi/Ga BEPR $\approx$ 0.5 and As/Ga BEPR $\approx$ 4.5.

However, sample II-1 does not follow the otherwise monotonic trend observed in the SEM-derived surface coverage. Therefore, a more detailed statistical analysis of the AFM maps was performed. When the total droplet volume is plotted as a function of As/Ga BEPR, an approximately linear decrease is obtained, as shown in Figure 27(a). The apparent discrepancy between the surface-area and volume trends can be explained by changes in the droplet composition, as observed in the EDX maps shown in Fig. 17, 22, and 26.

At low As/Ga BEPR, the surface features are mainly Ga-rich droplets. In the intermediate As/Ga BEPR range, biphasic Ga–Bi droplets become dominant, whereas at higher As pressure the droplets contain either pure Bi or Ga–Bi phases with a larger Bi-rich fraction. These compositional differences strongly influence the apparent droplet statistics. In particular, biphasic droplets typically consist of a taller Ga-rich region and a shallower Bi-rich region. As a result, although the cumulative droplet volume decreases with increasing As pressure, the surface coverage can remain relatively large up to As/Ga BEPR values of approximately 4 because the biphasic droplets are laterally wider and flatter.

The roundness of the droplets was also investigated, as shown in Figure 27(b). This parameter was found to be strongly correlated with droplet composition. For the mostly Ga-rich droplets formed at very low As/Ga BEPR, the roundness parameter is close to 1, and the diameter distribution resembles a nearly Gaussian distribution, as shown for sample I-3 in Figure 27(c). In contrast, increasing the As pressure leads to less circular features and a broader, more irregular diameter distribution, as shown for sample II-1 in Figure 27(d). This behaviour is consistent with the formation of biphasic droplets. For samples grown with As/Ga BEPR > 4, the roundness also depends on the supplied Bi flux, with higher Bi flux resulting in less circular surface features.

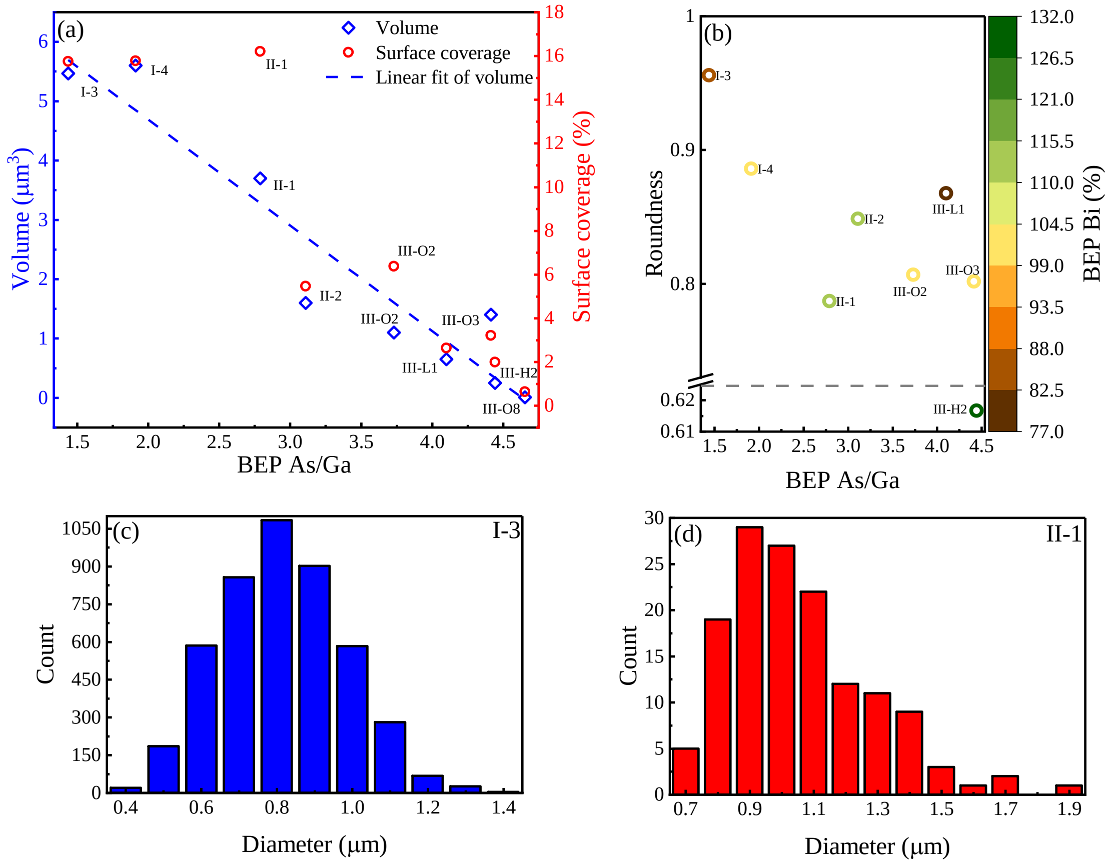

Fig. 27. (a) Total droplet volume, extracted from AFM images, as a function of As/Ga BEPR (left y-axis, blue). The dotted line shows a linear fit to the volume dependence. The percentage of surface area covered by droplets, extracted from SEM image analysis, is shown on the right y-axis (red). (b) Droplet roundness, obtained from AFM images, as a function of As/Ga BEPR; the colour scale indicates the Bi BEP. Statistical distributions of droplet diameters obtained from SEM images are shown for samples I-3 and II-1 in panels (c) and (d), respectively.

3.3 Defining the Optimal Windows

Taking everything into account, we can summarize the samples from all four series into two application-ready growth condition windows I and III-O, while the series II, III-L, III-H, and IV show features not suitable for producing emitters. The full summary of the regions according to the relation between optical properties and growth conditions is summarized in Fig. 28.

Series III was found to be a reproducible growth window, with the possibility of achieving intense PL. Nevertheless, series III is highly sensitive to deviations from the optimal Bi flux, which results in reduced intensity and broader emission linewidth. Furthermore, series I generally exhibited narrower emission bands and weaker temperature-induced quenching than series III.

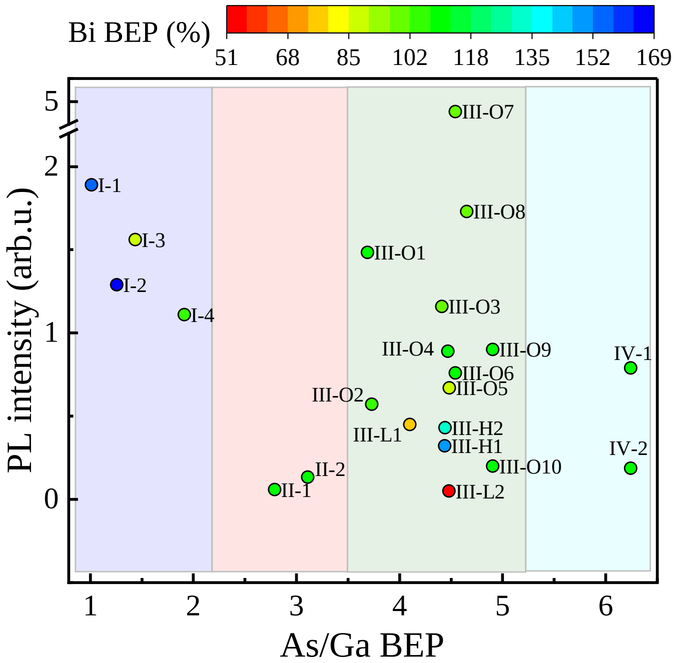

Fig. 28. PL peak intensity dependence on BEP As/Ga of samples grown for the whole layer investigation. The graph is split into series, blue - series I, red - series II, green - series III, and cyan - series IV. The color of the symbol denotes the Bi flux used, according to the legend above the plot.

These features make series I, a previously unexplored growth window, a possible candidate for high-emission-efficiency GaAsBi epitaxial layers. On the other hand, the structural and surface characterization shows that full-thickness layers could only be grown using BEP As/Ga values of approximately 4.4 and higher. This is expected, since at lower values As becomes the species limiting the growth rate. This is further supported by the fact that the volume of metallic unincorporated material on the sample surface scaled linearly with the change in As flux. Nonetheless, the surface features of series I were attributed to Ga accumulation. Therefore, according to the critical Ga-coverage mechanism proposed in subsection 3.2.4, we suppose that good-crystalline-quality thin samples with moderate surface quality can be grown by limiting the growth time. Thus, the growth conditions of series I are suspected to be favorable for MQW growth. Subsequently, the device prototypes presented in the rest of this work were grown using these conditions.

3.4 Growth and Characterization of NIR Emitters

In this section NIR emitters grown by MBE are presented. The device properties were selected according to the task of an international project, of proposing a two-wavelength sensing solution for integrated pulse oximeters. The requirements for the devices were two narrow spectral line emitters, LDs, operating at 800 nm and 1100 nm. Since the device structures were meant for integration onto a Si-based platform, namely SiC, they were grown on an AlAs sacrificial layer used to remove the native substrate and transfer onto an integrated chip, using a transfer procedure described by *Geum et al.* [47]. The motivation behind the wavelength selection is briefly described in our earlier works [5,48]. To achieve the 800 nm emission, relatively classical designs utilizing GaAs/AlGaAs MQW active area, were produced. Since this is a mature technology for NIR sources, this also serves as a reference of device properties for a well-developed material system. For the 1100 nm wavelength GaAsBi/GaAs MQW active regions are used. Due to a more difficult control of the growth, for these emitters a range of 1000 to 1150 nm was used for optimization.

3.4.1 Optimization of the Quantum Well Active Region

Following the growth parameters used for series I of thick layer growth, the optimization of a GaAsBi/GaAs QW structure was performed. In the calibration steps the BEP As/Ga was kept in the range of 1 to 1.2, while a large Bi flux was supplied (BEP Bi/Ga > 0.8). When considering application-focused QW structures the main technological parameter is the substrate temperature. Here there are several temperature-related effects to consider. First, the high BEP Bi/Ga enables the fully temperature-limited regime. It was noticed in the investigation of GaAsBi layer series I, that large Bi flux does not cause deterioration of the optical and structural properties. Following these results a very large Bi flux was chosen, meaning that the substrate temperature control enables a very wide emission wavelength window. Using this method QW structures with central emission wavelength well in the O-band (longer than 1300 nm) were grown, and are shown in Fig. 29.

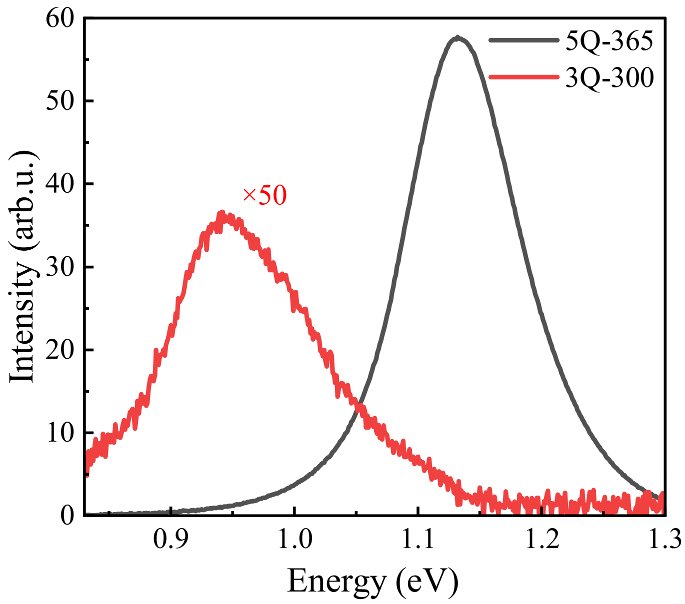

Fig. 29. RT PL spectra of GaAsBi MQW samples grown under the temperature-limited regime. The samples are named by the number of QWs (5 QWs (black curve) 3 QWs (red)), and the growth temperature used for the GaAsBi layer growth (365 °C) and (300 °C). The spectra of 3Q-300 is multiplied 50 times for clarity.

At the same time high emission intensity structures emitting at the target of around 1.13 eV could be realized. Moreover, we show that a structure emitting at 1 eV, around 1240 nm, retained a fully homogeneous PL signal on a full 2-inch substrate (see Fig. 30). This result shows that even at high Bi contents (estimated ≈ 7%Bi from PL), the structure is lattice mismatch dislocation free. In contrast, at such emission wavelengths, a quarter of a 2-inch InGaAs structure already shows signs of partial relaxation (see Fig. 2). The second important temperature related peculiarity is the growth of subsequent layers after the MQWs. The charge transport layers in both LEDs and LDs will be grown under elevated temperatures. For this reason the calibration samples are also capped by high temperature (HT) GaAs, to simulate the effects during the growth of a full diode. It was noticed in earlier works that the HT step results in a blue-shifted emission and increased intensity. The blue-shift is attributed to the redistribution and out-diffusion of Bi from the GaAsBi lattice, while the increased intensity is caused by the annihilation of point defects that were formed due to the low temperature (LT) growth. While these effects have to be taken into account in advance, both structures shown in Fig. 29 were grown with HT capping layers, showing the ability to control this phenomenon.

Elevated temperature also has a pronounced effect on the sample surface. The DIC pictures show typical surface views, of samples grown with and without the HT step (see Fig. 31). While both structures are free of metallic Ga droplets that formed under these conditions for layers in series I, this can be explained by the much lower thickness of the As-limited growth. Furthermore, the barriers are grown in As-rich conditions, during which the droplets can contribute to the growth of the actual GaAs alloy [49]. On the other hand, such growth still causes increased roughness. The sample with the HT step shows a better surface quality. This is attributed to an even larger increase of As flux during HT GaAs growth, in addition to the increased droplet mobility and surface diffusion.

In summary, this subsection demonstrates the ability to transfer the growth conditions of series I, to the growth of GaAsBi MQW structures. The structures exhibit a wide range of emission energies, obtained via the substrate temperature limited growth regime, moreover high intensity is seen for the MQW structure at the target emission wavelength. Finally, the surface quality of the structures is enhanced, when compared to layers discussed in section 3.2.4. The enhancement is attributed to the barrier growth in As-rich conditions, and the effects of elevated substrate temperature.

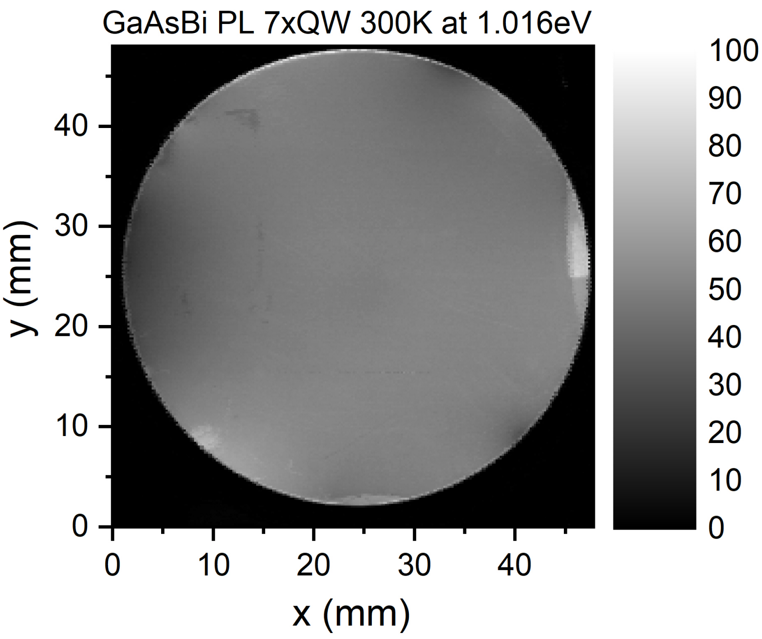

Fig. 30. RT PL mapping of a GaAsBi 7 x QW sample emitting at 1.016 eV. The sample is grown on a full 2 inch substrate. The map shows the ability to achieve good homogeneity over a large area, the absence of any perpendicular lines of reduced intensity confirms the absence of misfit dislocations.

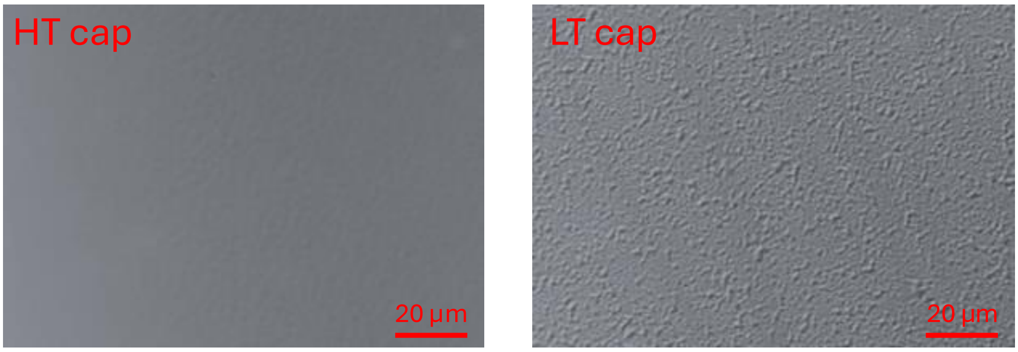

Fig. 31. DIC surface morphology comparison of samples with an HT (left) and LT (right) capping layer. An increased surface quality is seen on the HT capped sample.

3.4.2 GaAsBi Light Emitting Diodes

The initial part in producing GaAsBi-based electrically pumped emitters, was fabrication of LEDs. Transferring the growth technology to LEDs is a logical first step, as the initial characterization of such devices, requires minimal processing steps. Three types of device structures are considered in this section. The initial step was developing the technology of classical device architecture on AlAs sacrificial layer (nS-n). After that a device on p-type substrate was fabricated to provide a proof-of-concept for growing a structure in a non-standard way, starting from the p-doped layers (p-p). The necessity of such design, comes from application in integrated photonic circuits, where the transfer procedure effectively flips the device stack, and the top contact is mounted on the secondary substrate, which is usually n-type. The peculiarity in growing such structures is the Be (p-type dopant used for GaAs) diffusion under elevated temperatures [50]. Finally, a structure with both the flipped p-i-n design on sacrificial layer is realized (nS-p). The samples are named according to the structure, the first letter signifies the type of substrate, the capital S shows the presence of a sacrificial layer, while the letter after dash shows the bottom contact type.

The first, nS-n, structure was grown on a 350 μm thick n-type GaAs:Si substrate. First, a 500 nm thick AlAs sacrificial layer was deposited, followed by a 500 nm thick n-type GaAs:Si contact layer. The active region consisted of five 5.5 nm thick GaAsBi rectangular quantum wells separated by 7 nm thick GaAs barriers. The quantum well region was placed between GaAs spacer layers and capped with a 500 nm thick p-type GaAs:Be layer. The nominal carrier concentrations were 2×10^{18} cm^{-3} for the n-type GaAs:Si layer and 5×10^{18} cm^{-3} for the p-type GaAs:Be layer.

After growth, part of the structure was etched down to the n-type GaAs:Si layer in order to access both doped regions. Indium contacts were then formed on the n- and p-type GaAs layers, allowing the structure to be investigated by EL measurements.

Room-temperature EL spectra of the fabricated LED are shown in Figure 32. The structure exhibits clear emission from the GaAsBi active region with a peak energy of approximately 1.16 eV, corresponding to a wavelength of about 1070 nm. The emission position remains nearly unchanged over the investigated injection-current range, indicating stable operation of the active region under room-temperature electrical excitation.

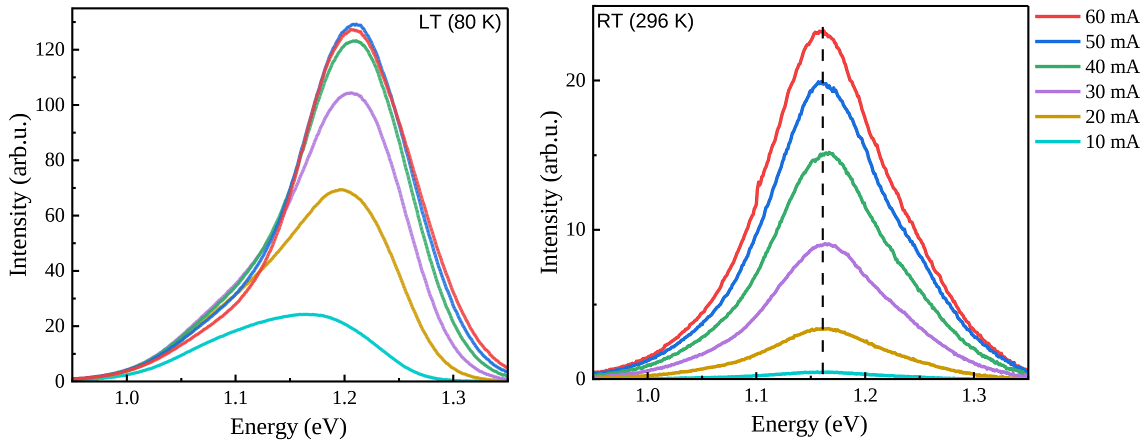

Fig. 32. Injection-current-dependent EL spectra of the LED nS-n measured at 80 K (left) and room-temperature (right). The legend indicating the injection current is common for both sets of spectra.

The same structure was also investigated at 80 K, as shown in Figure 32. At low temperature, the emission peak shifts to approximately 1.21 eV, corresponding to around 1025 nm at an injection current of 60 mA. A red-shift of the emission is observed when the injection current is reduced. This behavior is commonly associated with carrier localization effects in GaAsBi. At low temperature, holes can become trapped in localized states within the band gap and do not have sufficient thermal energy to escape. As the injection current is increased, these localized states are gradually filled, and the emission shifts towards higher energies, closer to the band-to-band transition [37].

The temperature dependence of the nS-n LED EL spectra was further investigated at a constant injection current of 50 mA. The spectra measured between 30 K and 300 K are presented in Figure 33 a), while the extracted peak-position dependence is shown in Figure 33 b). A secondary emission feature becomes visible mainly in the temperature range from 90 K to 210 K. This suggests that more than one radiative recombination path contributes to the emission. The most likely origin is a slight non-uniformity between the individual quantum wells, caused by differences in Bi content, well thickness, or interface quality.

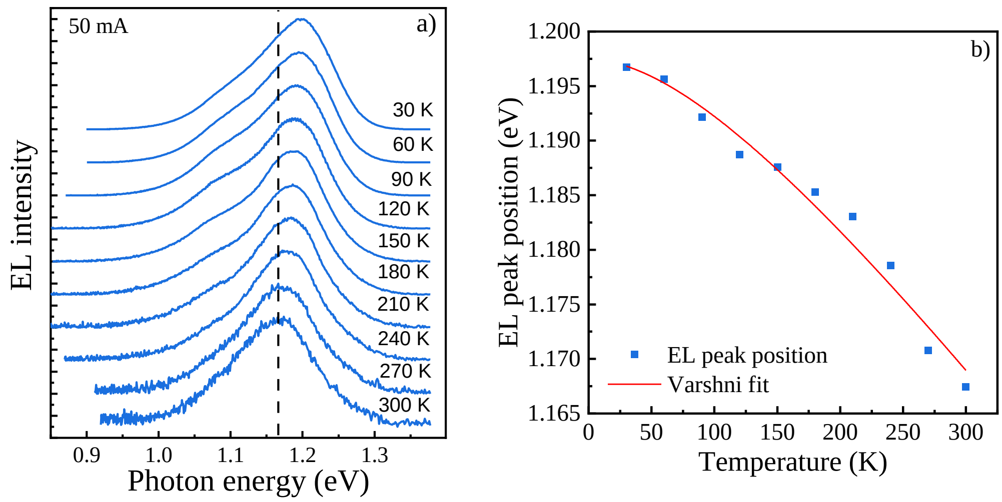

Fig. 33. (a) Temperature-dependent EL spectra of the GaAsBi LED measured at an injection current of 50 mA. (b) Temperature dependence of the EL peak position fitted using the Varshni relation.

Despite this additional spectral feature, the device shows good temperature stability, which is one of the characteristic advantages of GaAsBi-based emitters. Over the temperature range from 30 K to 300 K, the EL peak shifts by only 29 meV, corresponding to approximately 27 nm. Therefore, the fabricated GaAsBi LED demonstrates stable electrically pumped emission in the near-infrared spectral range and confirms the suitability of the optimized GaAsBi quantum well active region for device fabrication.

The other two devices were grown to test the technological feasibility of growing untraditional, flipped diode structures. The main challenge in growing such devices is the Be diffusion. To limit this, all of the growth was carried out at a lower temperature of no more than 500 °C.

The first device grown for this investigation was an LED on a p-type GaAs:Zn substrate (p-p). This is the simplest structure to test, as the substrate itself acts as the first p-type contact layer, while the n-type contact can be soldered on the surface of GaAs:Si. An identical, 5×QW GaAsBi/GaAs, active region to the previous LED was used. Another obstacle in growing on p-type substrate is the temperature measurement. Accurate band-edge thermometry could not be applied due to the high p-type carrier concentration in the GaAs:Zn substrate, which is larger than 1×10^{19} cm^{-3}. For this reason, the temperature was estimated from the thermocouple, by subtracting the previously calibrated value of around 70 °C, to obtain an estimate of the actual substrate temperature.

Room-temperature EL was observed from p-p, confirming electrically pumped emission from the GaAsBi QW active region. The spectrum measured at an injection current of 95 mA is shown in Figure 34.

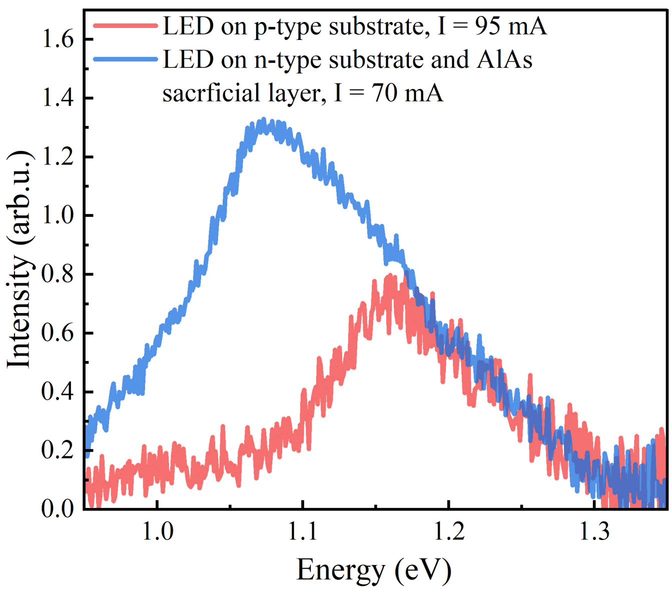

Fig. 34. Room temperature EL spectra of the GaAsBi LEDs p-p at 95 mA injection (red), and nS-p (blue) at 70 mA injection.

The emission peak is located at approximately 1.162 eV, corresponding to a wavelength of about 1066 nm. However, the spectrum is relatively noisy, indicating low emitted intensity. This reduced output is attributed to the combined influence of the lower quality and increased optical absorption of the p-type substrate, and the use of reduced-temperature growth for the doped GaAs layers.

The second structure, nS-p, was grown on an AlAs sacrificial layer deposited on an n-type GaAs:Si substrate. The use of the AlAs layer provides electrical and structural separation from the substrate and is intended for future substrate removal or transfer processes. Apart from the added sacrificial layer, the general LED design was kept similar to that of p-p, with the same GaAsBi 5×RQW active region placed between p- and n-type GaAs contact layers. In this case, the n-type substrate allowed more reliable temperature monitoring during growth, and the active region was grown at a calibrated temperature of approximately 350 °C.

The room-temperature EL spectrum of nS-p, measured at 70 mA, is shown in Figure 34. The emission peak is centered at approximately 1.072 eV, corresponding to about 1156 nm. The redshift compared with p-p indicates that a larger Bi fraction was incorporated into the GaAsBi QWs. This difference is most likely caused by the lower actual growth temperature of the active region in nS-p, while the emission energy of p-p may have been shifted by uncertainty in the temperature calibration on the p-type substrate.

Although the emission from nS-p is broader, with a FWHM of approximately 190 meV, the spectrum is noticeably less noisy than that of p-p. This suggests improved emission output despite the longer emission wavelength and therefore higher Bi content, which would normally be expected to increase defect-related losses. The result supports the conclusion that the p-type substrate had a significant negative effect on sample p-p.

Overall, both structures demonstrate room-temperature electroluminescence from GaAsBi QW active regions in flipped LED configurations. The structure grown directly on p-type GaAs:Zn confirms the simplest proof of concept, while the AlAs-based structure shows improved spectral quality and extends the emission wavelength to 1156 nm. However, the results also show that the low growth temperature required to limit Be diffusion remains a major limitation, as it degrades the quality of the doped layers and the active region.

The broader point illustrated by the investigation into LEDs is the proof of the technological capabilities of MBE growth of different device architectures. It was confirmed that GaAsBi electrically pumped emitters are stable in a wide temperature range, further the AlAs sacrificial layer itself proved to have no detrimental impact on the device parameters, illustrated by the LED nS-n. On the other hand, the peculiar growth of flipped devices was shown to have a negative impact on the device performance. The main cause is suspected to be the reduced growth temperature needed to suppress the Be diffusion, for sample p-p, an additional decrease in optoelectronic properties is attributed to the phenomena caused by the p-type substrate. Nevertheless, all structures discussed in this subsection showed EL signal at room-temperature, providing the basis of technology transfer to more complicated structures like LDs.

3.4.3 GaAsBi & AlGaAs Laser Diodes

In this subsection LDs fabricated using the developed technology are reviewed. To show the technological capabilities of producing application-oriented devices the section is started with a brief discussion on GaAs/AlGaAs devices meant for 800 nm emission and serving as a parameter reference point. Moreover, GaAsBi MQW based LDs are presented, showing both the ability to reach a target emission of around 1100 nm, and providing steps to increase the performance metrics by a more intricate, PQW-based active region and additional processing steps. All laser bars are formed following the same procedures, with a size of 5 x 500 μm, making their output characteristics directly comparable. The samples are named according to the active area design. The first letter indicates the barrier shape in the active region, R - for classical rectangular, P - where parabolic grading was used. The second two letters indicate the alloy used for QWs, Al - for AlGaAs system, Bi - for GaAsBi. In addition, one LD was fabricated with the flipped design, denoted as RBi-p. A similar general growth sequence was used for all five LD structures. The device stacks contained highly doped Si- and Be-doped n^+- and p^+-GaAs contact layers, with carrier concentrations above 2×10^{18} cm^{-3}, to ensure the formation of ohmic contacts. The active regions were surrounded by $Al_{0.5}Ga_{0.5}As$ cladding layers, doped in the range of $2{-}5 \times 10^{17}$ cm^{-3}, which were used for both carrier injection and optical confinement.

The growth of the GaAsBi-containing active regions required additional adjustments compared with the AlGaAs-based structures. Before depositing the GaAsBi quantum wells, the growth was interrupted in order to reduce the substrate temperature to the 350−370 °C range and to stabilise the As flux to ensure conditions close to those described previously, used for both the LEDs and series I layers. The GaAsBi quantum wells were grown under Bi-rich conditions, so the incorporated Bi content was governed mainly by the substrate temperature. For the structures prepared for substrate removal and transfer, a 1000 nm thick AlAs sacrificial layer was included below the diode stack. The main parameters of the structure are summarized in Table 2. First, two AlGaAs-based devices are fabricated aiming at an emission wavelength of 800 nm. The spectral and output power properties are presented in Fig. 35.

Table 2. Structural parameters of the intrinsic regions of the investigated laser diodes. Barrier composition denotes the barrier used in-between separate QWs in MQW gain regions. Outer barriers are the layers between the spacers and the first/last QW, inner barriers are the layers between a pair of QWs.

Laser diode	**RAl**	**PAl**	**RBi**	**PBi**	**RBi-p**
QW type	RQW	PGBs	RQW	RQW in PGBs	RQW
No. of QWs	2	1	3	3	3
QW composition	(Al,Ga)As			GaAsBi	
QW thickness (nm)	2	25	6.8	10	5.5
Parabolic grading	–	$Al_{0.30} \leftrightarrow Al_{0.09}$	–	$Al_{0.30} \leftrightarrow Al_{0.00}$	–
Barrier composition	$Al_{0.15}Ga_{0.85}As$	–	GaAs	GaAs	GaAs
Outer/inner barrier thickness (nm)	5 / 10	–	– / 7	– / 10	– / 7
Spacer composition	$Al_{0.30}Ga_{0.70}As$	$Al_{0.30}Ga_{0.70}As$	GaAs	–	GaAs
Spacer thickness (nm)	200	200	25	–	25

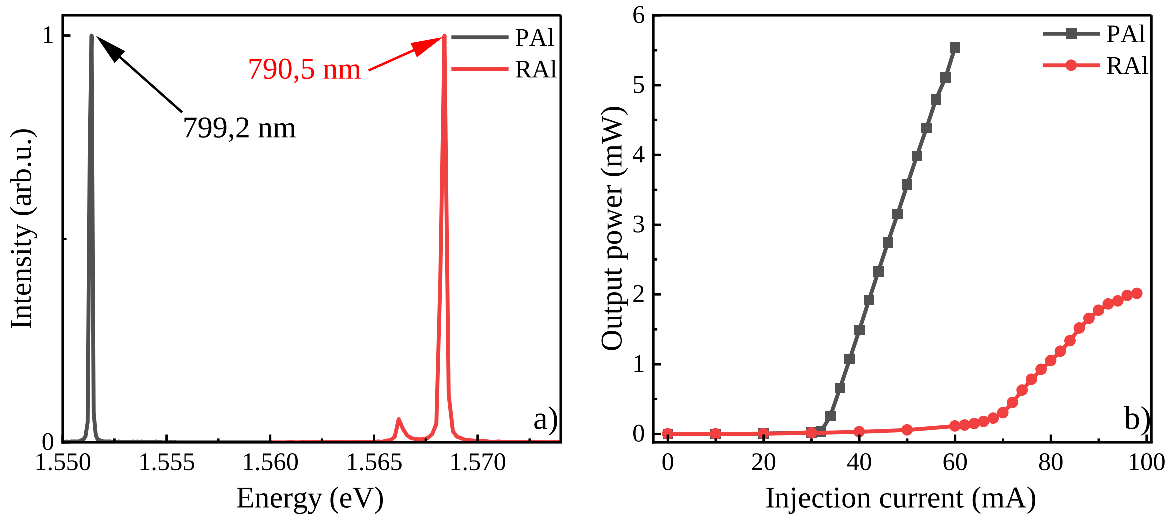

Fig. 35. a) Room-temperature lasing spectra of AlGaAs-based LDs RAl and PAl (left). b) The output power versus injection characteristics of both LDs measured via CW injection at the temperature of 20.6 °C for PAl and 22.7 °C for RAl.

The major difference between the two devices shown is the active region design. In the laser RAl the gain region is comprised of two $Al_{0.06}Ga_{0.94}As$ 2nm thick QWs separated by $Al_{0.15}Ga_{0.85}As$ 10 nm thick barrier. On the other hand, LD PAl had a rather exotic active area design consisting of a single PQW. The parabolic grading was realized by gradually decreasing the Al content every 4 monolayers, starting from 30 % Al, reaching 9 %, and returning back to 30 %. Such structure was expected to enhance the laser performance, since earlier investigations, showed an increase in PL intensity attributed to better carrier trapping efficiency [31]. In this work, a positive effect on the lasing by electrical injection was also noticeable. The LD PAl, had a considerably lower lasing threshold (I_{th} = 33 mA), and a higher maximum output power of more than 5.5 mW at 60 mA. On the contrary, for the structure RAl I_{th} was 66 mA. Furthermore, the power versus injection curve showed signs of saturation at 90 mA, and the maximum recorded power was 2 mW at 98 mA.

With the initial results on AlGaAs-based lasers, we moved to transferring the GaAsBi growth technology into laser diodes. All GaAsBi lasers were pumped using pulsed electrical injection of 50 ns pulses at 1 kHz frequency. The output powers discussed are the peak powers of a single pulse. We begin with testing the technological capability of flipped diode structure in LDs by fabricating the RBi-p laser. Even though lasing from the structure was registered at ≈1014 nm, the emission line was considerably wider than all other lasers. The output power was low and unstable, preventing a representative measurement. It is suspected that this is influenced by the same effects discussed for LEDs, namely Be diffusion and reduced growth temperature.

The sample RBi was the only laser structure grown on an AlAs sacrificial layer. Otherwise the classical design was selected for this structure, with p-type contact on the top. The growth conditions were optimized to achieve an emission line close to the target wavelength, at 1107 nm. Furthermore, an output power was registered at 9.4 mW (I=3 A), with an I_{th} of around 2.5 A.

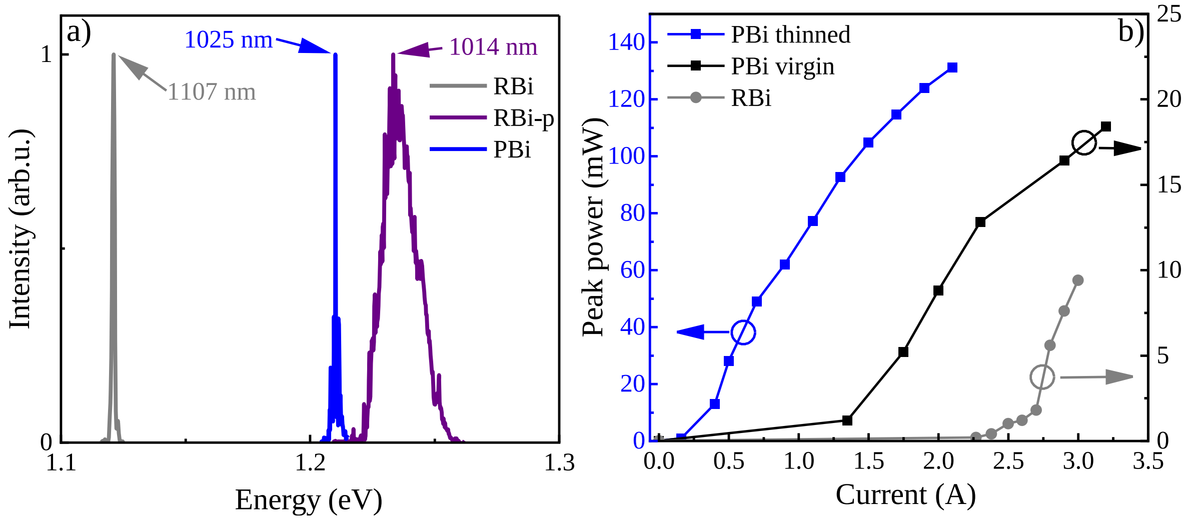

Fig. 36. a) Room-temperature lasing spectra of GaAsBi-based LDs RBi, RBi-p, and PBi. b) The output versus injection current characteristics of LDs RBi and PBi measured via pulsed injection (50 ns at 1 kHz), RBi (gray) and PBi virgin (black) curves are obtained from lasers without substrate thinning, while the blue curve of PBi thinned shows the enhanced characteristics after thinning.

The next step was applying all of the before mentioned growth and structural optimization steps, to achieve a near-optimal structure in terms of I_{th} and output power. A GaAsBi MQW active region, containing three QWs, was sandwiched between parabolically graded barriers. This design already showed around two times higher power and lower I_{th}, when comparing LD RBi and PBi. A further step was substrate thinning, which allowed to improve thermal properties and reduce the number of substrate defects affecting the injected current. This final step proved to be successful, as the laser structure with a I_{th} of as low as 0.25 A, was capable of 130 mW of output power at 1025 nm with 2 A of injection current.

All fabricated structures indicate a perspective direction for GaAsBi-based emitters. The work demonstrated control of the emission wavelength through temperature-limited growth, the ability to grow integration-ready structures on AlAs sacrificial layers, and the feasibility of flipped diode architectures. Starting from the investigation of GaAsBi thick layers in subsection 3.2, the growth of the alloy was better understood and series I was identified as a promising window for device fabrication. When this window was applied to QW growth, the temperature-limited regime was shown to be an effective way to control the emission wavelength over a wide spectral range. The investigation of LEDs confirmed the technological capability of producing different diode architectures. Finally, these results led to the demonstration of GaAsBi-based LDs, where the newly identified growth window was combined with an advanced parabolic active-region design, bringing GaAsBi emitters closer to application-relevant performance in NIR systems.

Conclusions

GaAsBi layer growth

1. The extended GaAsBi layer-growth study, focused on optimization for emission in the 1000–1200 nm range, showed that the alloy does not have a single universal optimum growth window. Instead, the growth behaviour is governed by different competing mechanisms depending on the As/Ga BEPR:

    - Bi incorporation is suppressed under As-rich (BEPR > 5) conditions;
    - near-stoichiometric regime (BEPR $\approx$ 4.5) is suitable for growing nominal-thickness GaAsBi layers with good surface morphology and a homogeneous thick layer composition. Although, small deviations away from optimal Bi flux have detrimental impact on both surface and optical properties;
    - the As-limited regimes showed that reduced As supply changes the standard GaAsBi growth mechanism. In the As/Ga BEPR range of 2–3.5, reduced growth rate, poorer optical quality, and Bi-rich nanoparticle formation is observed;
    - at BEP As/Ga values below 2, stronger group-V limitation causes Ga accumulation and a double-composition layer structure, where an initially formed Bi-rich region is followed by a lower-Bi-content material is grown due to Ga accumulation. Nonetheless, this regime produces GaAsBi with narrower and stronger room-temperature emission, combined with a weaker temperature-induced PL quenching, making it promising for thin GaAsBi layers and QW-based active regions.

GaAsBi QW and device structures

2. The low As/Ga BEP (1 to 1.2) growth regime identified from layer growth was applied to GaAsBi QWs. Under Bi-rich and As-limited conditions, temperature-limited growth was realized, proving the applicability of group-V limited growth for GaAsBi quantum structures.

3. GaAsBi LED structures grown in several configurations, including standard, flipped, and AlAs-sacrificial-layer designs exhibited Room-temperature EL in the application-relevant NIR range, with emission extending from approximately 1066 nm to 1156 nm.

4. Laser diode structures based on AlGaAs and GaAsBi active regions were fabricated for the two target wavelength ranges required for reflectance-mode pulse oximetry. AlGaAs-based devices emitted near 800 nm, while GaAsBi-based devices reached the 1000-1100 nm range.

5. Parabolically graded barriers improved the performance of the investigated laser diodes. In GaAsBi-based structures, the threshold current was reduced from 2.5 A to 1.3 A compared with the rectangular QW design, while the optimized thinned structure reached a threshold current of 250 mA and peak output power above 130 mW, showing a tenfold improvement in both I_{th} and power, when compared to the classical design.

Publications Related to the Thesis

A list of co-authored scientific publications related to the development, optimization, and characterization of III-V quantum structures and near-infrared emitters.

1. M. Jokubauskaitė, G. Petrusevičius, **A. Špokas**, B. Čechavičius, E. Dudutienė, and R. Butkutė, "Effects of parabolic barrier design for multiple GaAsBi/AlGaAs quantum well structures," *Lithuanian Journal of Physics*, vol. 63, no. 4, pp. 264–272, 2023.

2. A. Štaupienė, A. Zelioli, **A. Špokas**, A. Vaitkevičius, B. Čechavičius, S. Stanionytė, S. Raišys, R. Butkutė, and E. Dudutienė, "Internal quantum efficiency of GaAsBi MQW structure for the active region of VECSELs," *Applied Physics Letters*, vol. 125, 221102, 2024.

3. A. Zelioli, J. Žuvelis, U. Cibulskaitė, **A. Špokas**, E. Dudutienė, A. Vaitkevičius, S. Stanionytė, B. Čechavičius, and R. Butkutė, "Optimization of AlGaAs barrier for InGaAs quantum wells emitting in the near infrared," *Lithuanian Journal of Physics*, vol. 64, no. 4, pp. 244–252, 2024.

4. J. Glemža, **A. Špokas**, A. Zelioli, M. Kamarauskas, A. Bičiūnas, B. Čechavičius, J. Spigulis, *et al.*, "Quality evaluation of NIR laser diodes for medical application using low-frequency noise characterization," *Infrared Physics & Technology*, vol. 147, 105794, 2025.

5. A. Vaitkevičius, **A. Špokas**, A. Zelioli, U. Cibulskaitė, A. Bičiūnas, E. Dudutienė, B. Čechavičius, M. Skapas, A. Čerškus, M. Talaikis, P. Baranowski, P. Wojnar, and R. Butkutė, "Segregation - driven formation of bismuth quantum dots in parabolic GaAsBi/AlGaAs quantum structures," *Surfaces and Interfaces*, vol. 68, 106586, 2025.

6. A. Zelioli, **A. Špokas**, B. Čechavičius, M. Talaikis, S. Stanionytė, A. Vaitkevičius, A. Čerškus, P. Wojnar, V. Deibuk, E. Dudutienė, and R. Butkutė, "Comprehensive investigation of emission homogeneity of InGaAs multiple quantum wells using spatially resolved spectroscopy," *Scientific Reports*, vol. 15, 32885, 2025.

7. **A. Špokas**, A. Zelioli, A. Bičiūnas, B. Čechavičius, J. Glemža, S. Pralgauskaitė, M. Kamarauskas, V. Bukauskas, J. Spigulis, Y.-J. Chiu, J. Matukas, and R. Butkutė, "Optimising (Al,Ga)(As,Bi) quantum well laser structures for reflectance mode pulse oximetry," *Micromachines*, vol. 16, no. 5, 506, 2025.

8. A. Štaupienė, M. Jokubauskaitė, A. Zelioli, **A. Špokas**, M. Skapas, B. Čechavičius, R. Butkutė, and E. Dudutienė, "Improving optical properties through growth temperatures and post-growth annealing in parabolic GaAsBi/AlGaAs quantum wells," *Journal of Alloys and Compounds*, 187230, 2026.

9. I. Pliaterytė, L. Dundulis, J. Glemža, S. Pralgauskaitė, J. Matukas, **A. Špokas**, A. Zelioli, M. Kamarauskas, A. Bičiūnas, B. Čechavičius, and R. Butkutė, "Low frequency noise spectroscopy of GaAsBi QW structures for NIR light sources," *Fluctuation and Noise Letters*, 2640004, 2026.

Santrauka

ELEKTRIŠKAI KAUPINAMŲ NIR GaAsBi EMITERIŲ TECHNOLOGIJOS OPTIMIZAVIMAS

Aivaras Špokas

Šiame darbe aptariamas GaAsBi auginimo technologijos optimizavimas ir jos pritaikymas artimosios infraraudonosios spinduliuotės emiteriams. Darbo pradžioje siekiama išsiaiškinti pagrindinių technologinių parametrų (auginimo temperatūros, As/Ga ir Bi/Ga srautų santykių) įtaką užaugintų struktūrų optinėms bei struktūrinėms savybėms.

Iki šiol dažniausiai buvo laikoma, kad geros kokybės GaAsBi galima užauginti tik esant beveik stechiometriniam Ga ir As srautų santykiui. Šiame darbe auginimo sąlygų intervalas buvo išplėstas ir identifikuoti keturi skirtingi augimo režimai. Stechiometrinis režimas buvo tinkamas storų GaAsBi sluoksnių auginimui. Šiomis sąlygomis užaugintos struktūros pasižymėjo geru atkartojamumu ir intensyvia fotoliuminescencijos emisija. Esant aukštesniam arseno srautui, Bi įterpimas į gardelę buvo blokuojamas, todėl toks režimas nėra tinkamas GaAsBi technologijai. Struktūros, užaugintos esant nežymiam arseno trūkumui, pasižymėjo mažu emisijos intensyvumu ir stipriai suprastėjusia paviršiaus kokybe.

Netikėtas rezultatas buvo gautas dar labiau mažinant arseno srautą. Bandiniai, užauginti naudojant As/Ga srautų santykį nuo 0,22 iki 0,45, pasižymėjo intensyvia emisija, siaura fotoliuminescencijos emisijos juosta ir mažesniu temperatūriniu intensyvumo gesimu. Šis labai svarbus rezultatas parodė, kad tokios sąlygos (anksčiau netyrinėtos) gali būti palankios plonų kvantinių struktūrų auginimui. Todėl ši technologija buvo perkelta elektriškai kaupinamų GaAsBi emiterių gamybai.

Darbe pristatyti skirtingų dizainų šviestukai ir lazeriniai diodai. Šviestukai buvo naudojami pirminiam technologijos pritaikymo patikrinimui. Taip pat ištirta galimybė užauginti komponentus, suderinamus su integracija ant SiC platformos. GaAsBi kvantinių duobių pagrindu pagaminti lazeriniai diodai pademonstravo lazeriavimą 1014-1107 nm bangos ilgių intervale, kaupinant impulsiniu režimu. Galiausiai, panaudojus visus darbo metu pasiektus optimalius rezultatus, nuo storų sluoksnių auginimo technologijos optimizavimo iki emiterių dizaino tobulinimo, buvo pasiektas 130 mW pikinės galios lazeriavimas iš GaAsBi lazerinio diodo, kurio slenkstinė srovė siekė 250 mA.

References

[1] S. Francoeur, M.-J. Seong, A. Mascarenhas, S. Tixier, M. Adamcyk, and T. Tiedje, Band gap of $GaAs_{1-x}Bi_x$, 0 < x < 3.6%, *Applied Physics Letters*, 06 2003, **82**, 3874–3876.

[2] K. Alberi, O. D. Dubon, W. Walukiewicz, K. M. Yu, K. Bertulis, and A. Krotkus, Valence band anticrossing in $GaBi_xAs_{1-x}$, *Applied Physics Letters*, 07 2007, **91**, 051909.

[3] K. Oe and H. Okamoto, New semiconductor alloy $GaAs_{1-x}Bi_x$ grown by metal-organic vapor phase epitaxy, *Japanese Journal of Applied Physics*, nov 1998, **37**, L1283.

[4] Y. Tominaga, K. Oe, and M. Yoshimoto, Low temperature dependence of oscillation wavelength in $GaAs_{1-x}Bi_x$ laser by photo-pumping, *Applied Physics Express*, jun 2010, **3**, 062201.

[5] A. Špokas, A. Zelioli, A. Bičiūnas, *et al.*, Optimising (Al, Ga)(As, Bi) quantum well laser structures for reflectance mode pulse oximetry, *Micromachines*, 2025, **16**, 506.

[6] R. D. Richards, F. Bastiman, C. J. Hunter, D. F. Mendes, A. R. Mohmad, J. S. Roberts, and J. P. David, Molecular beam epitaxy growth of GaAsBi using As2 and As4, *Journal of Crystal Growth*, 2014, **390**, 120–124.

[7] J. Puustinen, J. Hilska, and M. Guina, Analysis of GaAsBi growth regimes in high resolution with respect to As/Ga ratio using stationary MBE growth, *Journal of Crystal Growth*, 2019, **511**, 33–41.

[8] Ł. Gelczuk, J. Kopaczek, T. B. Rockett, R. D. Richards, and R. Kudrawiec, Deep-level defects in n-type GaAsBi alloys grown by molecular beam epitaxy at low temperature and their influence on optical properties, *Scientific Reports*, 2017, **7**, 12824.

[9] A. Štaupienė, A. Zelioli, A. Špokas, *et al.*, Internal quantum efficiency of GaAsBi MQW structure for the active region of VECSELs, *Applied Physics Letters*, 2024, **125**, 221102.

[10] I. P. Marko and S. J. Sweeney, Progress toward III–V bismide alloys for near- and midinfrared laser diodes, *IEEE Journal of Selected Topics in Quantum Electronics*, 2017, **23**, 1–12.

[11] C. A. Broderick, M. Usman, S. J. Sweeney, and E. P. O'Reilly, Band engineering in dilute nitride and bismide semiconductor lasers, *Semiconductor Science and Technology*, 2012, **27**, 094011.

[12] A. Zelioli, A. Špokas, B. Čechavičius, *et al.*, Comprehensive investigation of emission homogeneity of InGaAs multiple quantum wells using spatially resolved spectroscopy, *Scientific Reports*, 2025, **15**, 32885.

[13] A. Zelioli, Growth and investigation of A3B5 quantum structures for VECSELs., *Vilniaus universiteto leidykla*, 2025.

[14] T. Rockett, R. Richards, Y. Gu, F. Harun, Y. Liu, Z. Zhou, and J. David, Influence of growth conditions on the structural and opto-electronic quality of GaAsBi, *Journal of Crystal Growth*, 2017, **477**, 139–143.

[15] D. Dagnelund, J. Puustinen, M. Guina, W. M. Chen, and I. A. Buyanova, Identification of an isolated arsenic antisite defect in GaAsBi, *Applied Physics Letters*, 02 2014, **104**, 052110.

[16] B. Carter, V. Caro, L. Yue, C. Tait, and J. Millunchick, The effect of III:V ratio on compositional and microstructural properties of $GaAs_{1-x}Bi_x$ (001), *Journal of Crystal Growth*, 2020, **548**, 125815.

[17] Y. Tominaga, Y. Horita, Y. Takagaki, F. Nishiyama, M. Yukimune, and F. Ishikawa, Crystalline quality of $GaAs_{1-x}Bi_x$ grown below 250 °C using molecular beam epitaxy, *Applied Physics Express*, 2022, **15**, 045504.

[18] G. Vardar, S. W. Paleg, M. V. Warren, M. Kang, S. Jeon, and R. S. Goldman, Mechanisms of droplet formation and Bi incorporation during molecular beam epitaxy of GaAsBi, *Applied Physics Letters*, 01 2013, **102**, 042106.

[19] A. W. Wood, K. Collar, J. Li, A. S. Brown, and S. E. Babcock, Droplet-mediated formation of embedded GaAs nanowires in MBE $GaAs_{1-x}Bi_x$ films, *Nanotechnology*, 2016, **27**, 115704.

[20] J. A. Steele, R. A. Lewis, J. Horvat, *et al.*, Surface effects of vapour-liquid-solid driven Bi surface droplets formed during molecular-beam-epitaxy of GaAsBi, *Scientific Reports*, 2016, **6**, 28860.

[21] C. R. Tait, L. Yan, and J. M. Millunchick, Droplet induced compositional inhomogeneities in GaAsBi, *Applied Physics Letters*, 2017, **111**, 042105.

[22] V. Braza, T. Ben, D. Reyes, N. Bailey, M. Carr, R. Richards, and D. Gonzalez, Structural and optical characteristics of epitaxially grown AlGaAsBi on GaAs for potential application in ultra-low noise avalanche photodiodes, *Applied Surface Science*, 2025, **689**, 162473.

[23] D. F. Reyes, F. Bastiman, C. J. Hunter, D. L. Sales, A. M. Sanchez, J. P. R. David, and D. González, Bismuth incorporation and the role of ordering in GaAsBi/GaAs structures, *Nanoscale Research Letters*, 2014, **9**, 23.

[24] M. A. Stevens, K. A. Grossklaus, and T. E. Vandervelde, Strain stabilization of far from equilibrium GaAsBi films, *Journal of Crystal Growth*, 2019, **527**, 125216.

[25] X. Lu, D. A. Beaton, R. B. Lewis, T. Tiedje, and M. B. Whitwick, Effect of molecular beam epitaxy growth conditions on the Bi content of $GaAs_{1-x}Bi_x$, *Applied Physics Letters*, 05 2008, **92**, 192110.

[26] P. Ludewig, N. Knaub, W. Stolz, and K. Volz, MOVPE growth of Ga(AsBi)/GaAs multi-quantum well structures, *Journal of Crystal Growth*, 2013, **370**, 186–190.

[27] P. K. Patil, E. Luna, T. Matsuda, K. Yamada, K. Kamiya, F. Ishikawa, and S. Shimomura, GaAsBi/GaAs multi-quantum well LED grown by molecular beam epitaxy using a two-substrate-temperature technique, *Nanotechnology*, 2017, **28**, 105702.

[28] P. K. Patil, F. Ishikawa, and S. Shimomura, GaAsBi/GaAs MQWs grown by MBE using a two-substrate-temperature technique, *Journal of Alloys and Compounds*, 2017, **725**, 694–699.

[29] P. K. Patil, F. Ishikawa, and S. Shimomura, Bismuth flux dependence of GaAsBi/GaAs MQWs grown by molecular beam epitaxy using two-substrate-temperature technique, *Superlattices and Microstructures*, 2017, **106**, 50–57.

[30] E. Dudutienė, A. Jasinskas, S. Stanionytė, M. Skapas, A. Vaitkevičius, B. Čechavičius, and R. Butkutė, Impact of elevated GaAs barrier growth temperature on the homogeneity and photoluminescence of GaAsBi multiple quantum wells, *Materials Science in Semiconductor Processing*, 2025, **199**, 109828.

[31] S. Pūkienė, M. Karaliūnas, A. Jasinskas, *et al.*, Enhancement of photoluminescence of GaAsBi quantum wells by parabolic design of AlGaAs barriers, *Nanotechnology*, aug 2019, **30**, 455001.

[32] P. Ludewig, N. Knaub, N. Hossain, *et al.*, Electrical injection Ga(AsBi)/(AlGa)As single quantum well laser, *Applied Physics Letters*, 06 2013, **102**, 242115.

[33] I. Marko, P. Ludewig, Z. Bushell, *et al.*, Physical properties and optimization of GaBiAs/(Al)GaAs based near-infrared laser diodes grown by MOVPE with up to 4.4% Bi, *Journal of Physics D: Applied Physics*, 2014, **47**, 345103.

[34] X. Wu, W. Pan, Z. Zhang, *et al.*, 1.142 μm GaAsBi/GaAs quantum well lasers grown by molecular beam epitaxy, *ACS Photonics*, 2017, **4**, 1322–1326.

[35] X. Liu, L. Wang, X. Fang, *et al.*, Continuous wave operation of GaAsBi microdisk lasers at room temperature with large wavelengths ranging from 1.27 to 1.41 μm, *Photonics Research*, May 2019, **7**, 508–512.

[36] R. Lewis, D. Beaton, X. Lu, and T. Tiedje, $GaAs_{1-x}Bi_x$ light emitting diodes, *Journal of Crystal Growth*, 2009, **311**, 1872–1875.

[37] R. D. Richards, C. J. Hunter, F. Bastiman, A. R. Mohmad, and J. P. R. David, Telecommunication wavelength GaAsBi light emitting diodes, *IET Optoelectronics*, 2016, **10**, 34–38.

[38] Y. P. Varshni, Temperature dependence of the energy gap in semiconductors, *Physica*, 1967, **34**, 149–154.

[39] M. Masnadi-Shirazi, D. Beaton, R. Lewis, X. Lu, and T. Tiedje, Surface reconstructions during growth of $GaAs_{1-x}Bi_x$ alloys by molecular beam epitaxy, *Journal of Crystal Growth*, 2012, **338**, 80–84.

[40] J. Puustinen, *Epitaxy and Properties of GaAs(N)Bi Alloys*. Tampere University Dissertations - Tampereen yliopiston väitöskirjat, Tampere University, 2023.

[41] J. A. Morgan and G. M. Nathanson, Atom scattering from atomic surfactants: Collisions of argon with a dilute Bi:Ga solution, *The Journal of Chemical Physics*, 02 2001, **114**, 1958–1961.

[42] D. Fan, Z. Zeng, V. G. Dorogan, *et al.*, Bismuth surfactant mediated growth of InAs quantum dots by molecular beam epitaxy, *Journal of Materials Science: Materials in Electronics*, 2013, **24**, 1635–1639.

[43] R. Butkutė, G. Niaura, E. Pozingytė, *et al.*, Bismuth quantum dots in annealed GaAsBi/AlAs quantum wells, *Nanoscale research letters*, 2017, **12**, 436.

[44] A. Vaitkevičius, A. Špokas, A. Zelioli, *et al.*, Segregation-driven formation of bismuth quantum dots in parabolic GaAsBi/AlGaAs quantum structures, *Surfaces and Interfaces*, 2025, 106586.

[45] A. Krotkus, I. Nevinskas, and R. Norkus, Semiconductor characterization by terahertz excitation spectroscopy, *Materials*, 2023, **16**.

[46] J. N. Heyman, N. Coates, A. Reinhardt, and G. Strasser, Diffusion and drift in terahertz emission at GaAs surfaces, *Applied Physics Letters*, 12 2003, **83**, 5476–5478.

[47] D.-M. Geum, M.-S. Park, J. Y. Lim, *et al.*, Ultra-high-throughput production of III-V/Si wafer for electronic and photonic applications, *Scientific Reports*, 2016, **6**, 20610.

[48] J. Glemža, A. Špokas, A. Zelioli, *et al.*, Quality evaluation of NIR laser diodes for medical application using low-frequency noise characterization, *Infrared Physics & Technology*, 2025, **147**, 105794.

[49] X. Li, J. Wu, Z. M. Wang, B. Liang, J. Lee, E.-S. Kim, and G. J. Salamo, Origin of nanohole formation by etching based on droplet epitaxy, *Nanoscale*, 2014, **6**, 2675–2681.

[50] E. F. Schubert, J. M. Kuo, R. F. Kopf, H. S. Luftman, L. C. Hopkins, and N. J. Sauer, Beryllium delta doping of GaAs grown by molecular beam epitaxy, *Journal of Applied Physics*, 02 1990, **67**, 1969–1979.